Electromagnetic Dipole Moments of Fermions

Dissertation

zur
Erlangung der naturwissenschaftlichen Doktorwürde
(Dr. sc. nat.)

vorgelegt der

Mathematisch-naturwissenschaftlichen Fakultät

der

Universität Zürich

von

Matteo Fael

aus Italien

Promotionskomitee

Prof. Dr. Thomas Gehrmann
Dr. Massimo Passera
Prof. Dr. Stefano Pozzorini
Prof. Dr. Ferruccio Feruglio

Zürich, 2014

"The more important fundamental laws and facts of physical science have all been discovered, and these are so firmly established that the possibility of their ever being supplanted in consequence of new discoveries is exceedingly remote ...
... our future discoveries must be looked for in the sixth place of decimals."

A. A. Michelson, in "Light Waves and Their Uses",
University of Chicago Press (1903), pp 23-25

Abstract

The electric dipole moment (EDM) and the anomalous magnetic moment ($g-2$) are physical observables sensitive to quantum corrections induced by the virtual particles that populate the vacuum. For this reason they are well suited to test the Standard Model (SM) of particle physics and to unveil unknown New Physics (NP) hidden at high energy. The electron and muon $g-2$ have been measured with the wonderful precision of 0.24 ppb and 0.54 ppm and they agree with SM prediction at the level of 1.3 and 3.7 standard deviations, respectively. They represent two of the most precise tests of the SM and greatest achievements in Quantum Field Theory.

In spite of that, the SM is insufficient to explain well-establish observations in various fields of physics: the nature of dark matter and dark energy, the cosmological inflation, the neutrino oscillations and their masses, the strong CP problem, the naturalness of the SM and the origin of matter-antimatter asymmetry. All of these call for NP that should lie at a mass scale higher that the electroweak scale.

Since the NP contribution to the dipole moments of a fermion is expected to scale with the square of its mass, from the theoretical point of view the dipole moments of heavy particles, such as the top quark or the tau lepton, are much more sensitive to NP effects than the electron or muon ones. However their very short lifetime makes it impossible to directly measure their electromagnetic properties, but indirect information may be obtained by precisely measuring cross sections and decay rates in processes involving the emission of a real photon by the heavy fermion.

In this thesis we investigate the possibility to determine the anomalous magnetic moment and the electric dipole moment of the top quark, in single-top-plus-photon production at the LHC, and tau lepton, in radiative leptonic tau decays at future high luminosity B-factories.

Abstract

Il momento di dipolo elettrico elettrico (EDM) e il momento magnetico anomalo ($g-2$) sono osservabili fisiche sensibili alle fluttuazioni quantistiche indotte dalle particelle virtuali che popolano il vuoto. Per questo motivo, essi sono particolarmente adatti a testare il Modello Standard (SM) della fisica delle particelle e a svelare possibile Nuova Fisica (NP) ad alta energia. I $g-2$ dell'elettrone e del muone sono stati misurati con la meravigliosa precisione di 0.24 ppb e 0.54 ppm e sono in accordo con la predizione del SM al livello di 1.3 e 3.7 deviazioni standard. In larga parte, rappresentano uno dei più precisi test del SM e una delle maggiori conquiste della Teoria dei Campi.

Nonostante ciò, il SM è insufficiente per spiegare molte consolidate osservazioni in vari campi della fisica: la natura della materia oscura ed energia oscura, l'inflazione cosmologica, le masse dei neutrini, la naturalezza dei parametri nel SM e l'origine dell'asimmetria materia-antimateria. Tali osservazioni richiedono NP a una scala maggiore della scala elettrodebole.

Poiché contributi di nuova fisica ai momenti di dipolo di una particella scalano con il quadrato della sua massa, i dipoli dei fermioni pesanti, come il leptone tau e il quark top, sono, da un punto di vista teorico, molto più sensibili ad effetti di nuova fisica rispetto quelli dell'elettrone o del muone. Tuttavia, la loro breve vita media rende difficile la misura diretta di queste proprietà elettromagnetiche. Quindi, tali informazioni devono essere ottenute indirettamente a partire dalla misura di sezioni d'urto e larghezze di decadimento in processi che coinvolgono l'emissione di un fotone reale da parte della particella pesante.

In questa tesi dunque, viene studiata la possibilità di misurare il momento magnetico anomalo e il momento di dipolo elettrico del quark top, in produzione di single-top a LHC, e del leptone tau, nei suoi decadimenti radiativi alle future B-factory ad alta luminosità.

Zusammenfassung

Das elektrische Dipolmoment (EDM) und das anomale magnetische Moment ($g-2$) erlauben Rückschlüsse auf die Quantenkorrekturen, die von virtuellen Teilchen, die das Vakuum bevölkern, induziert werden. Diese physikalischen Observablen sind daher gut geeignet, das Standardmodell (SM) der Teilchen zu testen und unbekannte Neue Physik (NP) bei hohen Energien zu entdecken. Der Wert von ($g-2$) für das Elektron und das Muon wurde mit der außergewöhnlichen Präzision von 0.24 ppb und 0.54 ppm gemessen. Die beiden Werte stimmen mit den Vorhersagen des Standardmodells innerhalb von 1.3 beziehungsweise 3.7 Standardabweichungen überein. Diese Ergebnisse zählen zu den präzisesten Tests des SM und zu den größten Erfolgen der Quantenfeldtheorie.

Das SM reicht jedoch nicht aus, um einige wohlbekannte Beobachtungen in verschiedenen Bereichen der Physik zu erklären: Die Natur von dunkler Materie und dunkler Energie, die kosmologische Inflation, Neutrinooszillationen und Neutrinomassen, das CP Problem der starken Wechselwirkung, die Natürlichkeit des SM und den Ursprung der Materie-Antimaterie Asymmetrie. All diese Beobachtungen lassen auf NP auf Skalen jenseits der elektroschwachen Skala schließen. Es wird erwartet, dass die Beiträge der NP zu den Fermiondipolmomenten proportional zum Quadrat der Masse des Fermions anwachsen. Daher sind von einem theoretischen Standpunkt aus betrachtet die Dipolmomente von schweren Fermionen, wie das des Topquarks oder des Tauleptons, viel sensitiver für Effekte der NP als die Dipolmomente des Elektrons oder des Muons. Die kurze Lebenszeit dieser Teilchen erlaubt es jedoch nicht, ihre elektromagnetischen Eigenschaften direkt zu messen. Es ist allerdings möglich, indirekt Informationen abzuleiten mittels der präzisen Messung der Wirkungsquerschnitte und der Zerfallsraten in Prozessen, bei denen das schwere Fermion ein reelles Photon emittiert.

In dieser Doktorarbeit untersuchen wir die Möglichkeit, das anomale magnetische Moment und das elektrische Dipolmoment des Topquarks und des Tauleptons zu bestimmen. Für ersteres werden Prozesse mit nur einem Topquark und einem Photon am LHC untersucht, für zweiteres werden radiative leptonische Tauzerfälle in zukünftigen B-Fabriken mit hoher Luminosität betrachtet.

Acknowledgements

I would like to express my sincere gratitude to my advisors, Thomas Gehrmann and Massimo Passera, for their continuous support over the past three years and valuable guidance, scholarly inputs and encouragements received throughout the research work. This joint doctoral project has been a wonderful possibility to be involved, at the same time, in two of the most fascinating and dynamic research fields in particle physics.

I also thank my experimentalist colleagues, Simon Eidelman and Denis Epifanov, for all the nice discussions and fruitful collaboration, and for providing me with the precious and detailed description of their work.

For many useful insights and interesting discussions throughout these three years I thank R. Frederix, M. Grazzini, A. Papaefstathiou, P. Paradisi, S. Pozzorini, D. Tommasini, R. Torre, P. Torrielli, J. Zurita and all the group of Ph.D. students in Padova and in Zurich. I also thank T. Lübbert, C. Duhr, D. Potter, and many others, for a lot of Doppelkopf and dinners at *Incrocio*.

My doctorate training and research have been supported by the University of Padova and the LHCPhenonet Initial Training Network. Also INFN, Sezione di Padova, and University of Zurich supported my participation to various schools and conferences.

There are no words to express the gratitude to my parents for their silent help and support: none of what I achieved would have been possible without them. Finally, thanks to Elisa, for the warm love and energy she gives to my life.

Contents

To Elisa

Introduction

The electric dipole moment (EDM) and the anomalous magnetic moment ($g-2$) are physical observables sensitive to quantum corrections induced by the virtual particles that populate the vacuum. Indeed, they are well suited to test the Standard Model (SM) of particle physics and to unveil unknown New Physics (NP) hidden at high energy. The electron and muon $g-2$ have been measured with the wonderful precision of 0.24 ppb [1] and 0.54 ppm [2] and they agree with SM prediction at the level of ~ 1.3 [3] and ~ 3.7 [2] standard deviations, respectively. They represent two of the most precise tests of the SM and greatest achievements in Quantum Field Theory. In spite of that, the SM is insufficient to explain well-established observations in various fields of physics: the nature of dark matter and dark energy, the cosmological inflation, neutrino oscillations and their masses, the strong CP problem, the naturalness in the SM and the origin of matter-antimatter asymmetry. All of these call for new physics that should lie at a mass scale higher than the electroweak scale.

In a large class of models beyond the SM, NP contributions to the $g-2$ of a particle are expected to scale as [3–6]

$$a_f^{\text{NewPhysics}} = C\left(\frac{m_f}{\Lambda}\right)^2, \tag{1}$$

where C could be of $\mathcal{O}(1)$ or smaller, and Λ is the mass scale associated to the NP. So for example, from a pure theoretical point of view, the $g-2$ of tau lepton is much more sensitive to NP effects than the muon and electron ones. Also, in view of its large mass, the top quark is even better suited to unveil deviations from the SM and to probe the dynamics that breaks the electroweak gauge symmetry. Furthermore, compared to the other quarks, the properties of the top are not spoiled by low-energy QCD effects since the top quark decays before hadronizing.

EDM interactions violate parity and time reversal, so that if CPT is a good symmetry, T violation implies CP violation and vice versa. The SM values for lepton and quark fundamental EDMs are astonishingly small, too tiny to be seen by the projected future experiments. Hence, the observation of a non-vanishing fundamental EDM would be bright evidence for a CP-violating NP effect [7, 8].

However, a very short lifetime poses many difficulties for the experimental determination of dipole moments so that indirect bounds have to be obtained in an indirect way through precise measurements of cross sections and decay widths. Several studies have established photon radiation in top pair production at hadron colliders as potential probe of anomalous coupling effects [9], which could be improved upon only at a future high-energy electron-positron collider [10]. Indeed, while indirect limits on anomalous electromagnetic couplings from electroweak precision data or flavor physics observables turn out to be very constraining for bottom quarks [11–13], only loose bounds can be obtained in the case of top quarks [14, 15].

In this thesis we propose single-top-plus-photon production as a tool to investigate the $tt\gamma$ coupling at the LHC. Indeed, with the cross sections for top pair production and single-top production being of comparable magnitude at this hadron collider, it appeared worthwhile to extend the $t\bar{t}\gamma$ production analysis in [9] to photon radiation in single top quark production. We analyze in detail signal and background processes contributing to single-top-plus-photon production (Secs. 2.4 and 2.5) and quantify the numerical magnitude of the top dipole moments that can be detected in the upcoming 14 TeV runs at the LHC (Sec. 2.6). In the end, we will give compelling reasons to analyze single-top-plus-gamma at the LHC by demonstrating that the bounds that can be obtained from single-top-plus-photon production are very much comparable in magnitude to those that can be obtained from $t\bar{t}\gamma$ final states. These channels are completely independent from each other and therefore can be further combined. In particular, we will show that existing bounds may be improved upon by up to one order of magnitude.

High luminosity B- and τ/charm-factories offer new opportunities in tau precision physics thanks to their high statistics and energy resolution. In particular, concerning the study of dipole moments at B-factories, in Ref. [16] it has been proposed to search for the tau anomalous magnetic moment form factor in tau pair production at the Υ resonances. However the beam energy spread at Belle and future Belle-II makes it very difficult to resolve these narrow resonances in the $\Upsilon \to \tau^+\tau^-$ decay channel (see Sec. 1.5).

For this reason we suggest in this thesis (Sec. 1.6) an alternative measurement of the tau anomalous magnetic moment via leptonic radiative decays $\tau \to l\nu_\tau\bar{\nu}_l\gamma$ with a precision of $\mathcal{O}(10^{-3})$, which is the same order of magnitude of the SM leading contribution to a_τ. In fact, the direct determination of the tau $g-2$, by measuring its spin precession as in the muon experiment, has so far been impossible and the present resolution on its anomalous magnetic moment [17] is more than an order of magnitude larger than its SM prediction [18].

Without the need to employ any low-energy QCD approximation, the proposed study of leptonic radiative decays offers the clean theoretical environment required by the desired experimental precision. To provide the theoretical framework for such measurements at $\mathcal{O}(10^{-3})$, we compute the polarized differential decay rate at NLO in the SM, including also the W-boson propagator effects and possible non-vanishing $g-2$ and EDM contributions (see Secs. 1.8 and 1.9). To the leading order in G_F but to all orders in α, the radiative corrections to muon decay are finite in the Fermi V-A theory after mass and charge renormalization. Since this special feature holds also for taus decaying into leptons, we calculate all NLO corrections to radiative leptonic decays in the Fermi theory, including full mass dependence.

The obtained prediction for the differential decay rate for $\tau \to l\nu_\tau\bar{\nu}_l\gamma$ is used in a dedicated feasibility study, where the whole data sample collected at Belle and the one planned at Belle II experiment are analyzed in order to establish which are the future achievable sensitivities to the tau dipole moments in radiative leptonic decays (Sec. 1.11). We will show that the measurement of the tau anomalous magnetic moment at Belle II can be already competitive with the current bound from DELPHI experiment [17], while the expected sensitivity to the tau EDM is still worse than the most precise measurement done at Belle [19].

Chapter 1

The determination of tau lepton dipole moments in radiative decays

1.1 Introduction

The current experimental determination of the tau anomalous magnetic moment is quite poor. The SM prediction of a_τ, presented in Sec. 1.3, is known with a precision of $5 \cdot 10^{-8}$ [18], while the bound coming from the DELPHI analysis of $e^+e^- \to e^+e^-\,\tau^+\tau^-$ cross section at LEP2 is only of $\mathcal{O}(10^{-2})$ [17], not even the order of magnitude of the leading contribution to a_τ, $\alpha/(2\pi) \sim 0.0011$. Also in the case of the tau EDM, the current sensitivity is similar, $|d_\tau| < 10^{-17}\, e{\cdot}\text{cm}$ [19] or $|d_\tau| < 10^{-3}$ if expressed in natural units of m_τ, to be compared with the small SM prediction $d_\tau \sim 10^{-35}\, e{\cdot}\text{cm}$ (see Sec. 1.4). In fact, fundamental EDMs are to such an extent below the current experimental capabilities that so far there has been no experimental evidence of any permanent electric dipole moment of elementary particle, nucleus, or atom. Therefore, the observation of a nonzero EDM would directly reveal the existence of a new source of CP violation not related to the SM.

Several methods have been advanced to improve upon the existing bounds, see Sec. 1.5, either via direct interaction of taus with a strong magnetic field or by precisely studying production channels or decays of the tau. In this chapter we investigate the possibility to determine the tau dipole moments via its radiative leptonic decays and to probe these observables with a precision of $\mathcal{O}(10^{-3})$ or better. For this reason, we provide with the theoretical framework for such measurement at the same level of precision, by thus including, in the decay rate, radiative corrections at next-to-leading order (NLO)

in QED, of $\mathcal{O}(\alpha/\pi)$, and the non-negligible contribution from the W-boson propagator, of $\mathcal{O}(m_\tau^2/M_W^2) \sim 5\cdot 10^{-4}$ (see Secs. 1.8 and 1.9). The comparison of this NLO prediction to sufficiently precise data may allow to determine a_τ and d_τ possibly down to the level of $O(10^{-4})$. The obtained prediction for the $\tau^- \to l^- \bar{\nu}_l \nu_\tau \gamma$ differential decay rate is then used in a feasibility study where the sensitivity to a_τ and d_τ of the whole data sample collected at Belle and the one planned at the Belle II experiment is analyzed (Sec. 1.11).

1.2 General $ff\gamma$ coupling

It is useful for further discussion to recall the structure of the $ff\gamma$ coupling. The most general vertex function describing the interaction between two on-shell fermions f and a photon can be written in the form

$$\Gamma_\mu(q^2) = -ie\left\{\gamma_\mu\left[F_{1V}(q^2) + F_{1A}(q^2)\gamma_5\right] + \frac{\sigma_{\mu\nu}}{2m_f}q^\nu\left[iF_{2V}(q^2) + F_{2A}(q^2)\gamma_5\right]\right\}, \quad (1.1)$$

where e is the proton charge, m_f the mass of the fermion, $\sigma_{\mu\nu} = i/2\,[\gamma_\mu, \gamma_\nu]$ and q is the four-momentum of the off-shell photon. Eq. (1.1) is the most general expression that satisfies Lorentz invariance and the Ward identity, when it is sandwiched in $\overline{u}(p)\Gamma_\mu(q^2)u(p')$. The functions F_{1V} and F_{2V} are called, respectively, the Dirac and Pauli form factors. Their meaning in general is not physical, since they can show infrared divergences [20, 21], nontheless in the limit $q^2 \to 0$ they are physical and related to the static quantities

$$\begin{aligned} F_{1V}(0) &= Q_f, \\ F_{2V}(0) &= a_f\, Q_f, \\ F_{2A}(0) &= d_f\,\frac{2m_f}{e}, \end{aligned} \quad (1.2)$$

where Q_f is the charge of the fermion, a_f and d_f are, respectively, the anomalous magnetic moment and the electric dipole moment. The identity $F_{1V}(0) = Q_f$ is the charge renormalization condition. The electric dipole contribution $F_{2A}(q^2)$ violates the discrete symmetry of P (parity) and T (time reversal) [22–24] and therefore CP-invariance (if CPT is a good symmetry of nature). Indeed, EDM vanishes in any CP-conserving theory. Since we now know that both symmetries are violated in the SM by weak interactions, we should expect at some level $d_f \neq 0$ due to the SM loop effects.

It is illustrative also to combine the two (real) dipole moments, a_f and d_f, into a single complex dipole moment [4]:

$$c_f = a_f\frac{Q_f e}{2m_f} - id_f. \quad (1.3)$$

Thanks to this definition the dipole moment interactions in Eq. (1.1) can be recast, in the limit $q^2 \to 0$, as

$$C_R\,\sigma_{\mu\nu}q^\nu P_R + C_L\,\sigma_{\mu\nu}q^\nu P_L \tag{1.4}$$

where P_R and P_L are, respectively, the right- and left-handed chiral spinor projectors and $c_f = C_R = C_L^*$. It is also possible to consider a more general non-hermitian interaction, where the two coefficients are not related, i.e. $C_R \neq C_L^*$. In this case one renounces CPT invariance, so that this discrete symmetry can be tested by measuring C_R and C_L. Here we anticipate that in the feasibility study of tau dipole moments we will not impose any restriction on C_R and C_L, i.e. we assume a_τ and d_τ to be complex numbers.

We noted that in general direct production processes of the fermion f are not suited to disentangle the contributions from the CP-conserving magnetic dipole moment a_f and the CP-violating electric dipole moment d_f. As a matter of fact, production amplitudes will usually probe the modulus of the complex dipole moment, i.e. the combination

$$|c_f| = \sqrt{\left(a_f \frac{Q_f e}{2m_f}\right)^2 + d_f^2}, \tag{1.5}$$

whereas they are almost insensitive to the phase,

$$\tan(\varphi_f) = \frac{d_f}{a_f}\frac{2m_f}{Q_f e}, \tag{1.6}$$

that can be regarded as a measure of CP violation. Indeed, since CP violation is generally a tiny effect, the phases φ_f are all expected to be very small, except possibly in the case of a Dirac neutrino where the anomalous magnetic moment and electric dipole moment are both tiny.

1.3 The SM prediction of a_τ

In this section we briefly recall the SM prediction for the tau anomalous magnetic moment, a_τ, that is given by the sum of QED, electroweak (EW) and hadronic (HAD) terms (for a more exhaustive analysis we refer the reader to Refs. [18, 25]). All reported results were derived using the CODATA [26] recommended mass ratios,

$$m_\tau/m_e = 3477.48\,(57), \tag{1.7}$$

$$m_\tau/m_\mu = 16.8183\,(27). \tag{1.8}$$

The value for m_τ adopted by CODATA in ref. [26], $m_\tau = 1776.99\,(29)$ MeV, is based on the PDG 2002 results [27].

1.3.1 QED contribution

The QED part, $a_\tau^{\rm QED}$, arises from the subset of SM diagrams containing only leptons and photons. This dimensionless quantity can be cast in the general form [28]:

$$a_\tau^{\rm QED} = A_1 + A_2\left(\frac{m_\tau}{m_e}\right) + A_2\left(\frac{m_\tau}{m_\mu}\right) + A_3\left(\frac{m_\tau}{m_e}, \frac{m_\tau}{m_\mu}\right), \tag{1.9}$$

where m_e, m_μ, and m_τ are the electron, muon, and tau mass.

The term A_1, arising from diagrams containing only photons and tau, is mass and flavour independent. In contrast the terms A_2 and A_3 are functions of the indicated mass ratios and are generated by graphs including also electrons and muons. Each function A_i can be expanded as power series in α/π and computed order by order:

$$A_i = A_i^{(2)}\left(\frac{\alpha}{\pi}\right) + A_i^{(4)}\left(\frac{\alpha}{\pi}\right)^2 + A_i^{(6)}\left(\frac{\alpha}{\pi}\right)^3 + \cdots . \tag{1.10}$$

Only one diagram is involved in the evaluation of the one-loop contribution.

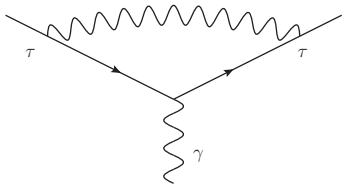

It provides the famous mass independent result of Schwinger [29]

$$a_1^{\rm QED} = \frac{\alpha}{2\pi}, \tag{1.11}$$

and so $A_1^{(2)} = 1/2$.

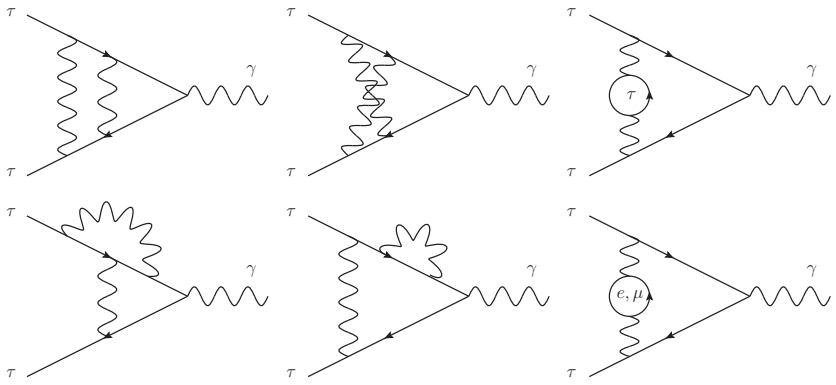

FIGURE 1.1: The QED two-loop corrections to a_τ. The mirror reflections of the fourth and fifth diagrams must be included as well.

At two-loop, see Fig. 1.1, seven diagrams contribute to the second order term $A_1^{(4)}$ and one to $A_2^{(4)}$. The mass independent term has the analytical expression [30]

$$A_1^{(4)} = \frac{197}{144} + \frac{\pi^2}{12} + \frac{3}{4}\zeta(3) - \frac{\pi^2}{2}\ln 2, \tag{1.12}$$

where $\zeta(z)$ is the Riemann zeta function. The coefficient of the two-loop mass-dependent contribution $A_2^{(4)}(1/x)$, with $x = m_e/m_\tau$ or m_μ/m_τ, is generated by the diagram with a vacuum polarization subgraph containing the virtual lepton e or μ. The exact result has the analytic compact form [31, 32]

$$\begin{aligned} A_2^{(4)}\left(\frac{1}{x}\right) = &-\frac{25}{36} - \frac{\ln x}{3} + x^2(4 + 3\ln x) + \frac{x}{2}(1 - 5x^2) \\ &\times \left[\frac{\pi^2}{2} - \ln x \ln\left(\frac{1-x}{1+x}\right) - \mathrm{Li}_2(x) + \mathrm{Li}_2(-x)\right] \\ &+ x^4\left[\frac{\pi^2}{3} - 2\ln x \ln\left(\frac{1}{x} - x\right) - \mathrm{Li}_2(x^2)\right], \end{aligned} \tag{1.13}$$

where $\mathrm{Li}_2(z)$ is the dilogarithm defined as

$$\mathrm{Li}_2(z) = -\int_0^z \frac{\ln(1-t)}{t} dt. \tag{1.14}$$

The numerical values for the fourth order A_i coefficients are reported in Tab. 1.1. Note that the errors are only due to the uncertainties of the mass ratios. The total fourth order contribution is

$$A_1^{(4)} + A_2^{(4)}(m_\tau/m_e) + A_2^{(4)}(m_\tau/m_\mu) = 2.057\,457\,(93). \tag{1.15}$$

term	value
$A_1^{(4)}$	$-\ 0.328\,478\ \cdots$
$A_2^{(4)}(m_\tau/m_e)$	$2.024\,284\,(55)$
$A_2^{(4)}(m_\tau/m_\mu)$	$0.361\,652\,(38)$

TABLE 1.1: numerical values for the fourth order A_i coefficients [33]

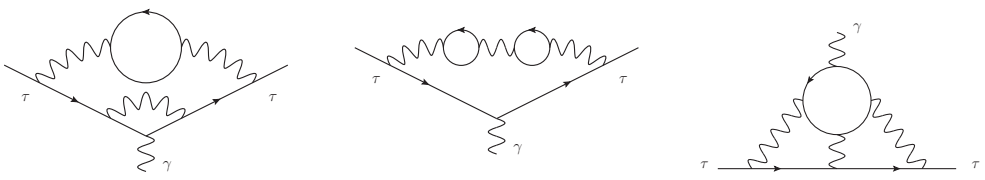

(A) Vacuum polarization type (B) Double vacuum polarization (C) Light-by-light

FIGURE 1.2: Some QED three loop diagrams contributions to a_τ.

More than one hundred diagrams contribute to the QED three-loop correction. The coefficient $A_1^{(6)}$ arises from 72 diagrams. Its exact expression is [34]

$$A_1^{(6)} = \frac{83}{72}\pi^2\zeta(3) - \frac{215}{24}\zeta(5) - \frac{239}{2160}\pi^4 + \frac{28259}{5184} + \frac{139}{18}\zeta(3) - \frac{298}{9}\pi^2\ln 2 + \frac{17101}{810}\pi^2 + \frac{100}{3}\left[\mathrm{Li}_4\left(\frac{1}{2}\right) + \frac{1}{24}(\ln^2 2 - \pi^2)\ln^2 2\right]. \tag{1.16}$$

The coefficients $A_2^{(6)}(m_\tau/m_i)$, $i = \mu, e$, can be further split into two parts: the first one $A_2^{(6)}(m_\tau/m_i, vac)$ receives contributions from 36 diagrams containing either electron or muon vacuum polarization loops (see for example Fig. 1.2a), whereas the second one, $A_2^{(6)}(m_\tau/m_i, lbl)$, is due to 12 light-by-light scattering diagrams with either electron and muon loops (see Fig. 1.2b). The coefficient $A_3^{(6)}$ arises from diagrams with two-loop vacuum polarization subgraphs. The values of three-loop coefficients are reported in Tab. 1.2. The errors are due to the mass ratio uncertainties (see the beginning of this section). Adding these results one finds:

$$\sum_i A_i^{(6)} = 57.9315\,(27). \tag{1.17}$$

term	value
$A_1^{(6)}$	$1.181\,241\,456\,\cdots$
$A_2^{(6)}(m_\tau/m_e)$	46.392 1 (15)
$A_2^{(6)}(m_\tau/m_\mu)$	7.010 21 (76)
$A_3^{(6)}(m_\tau/m_e,\ m_\tau/m_\mu)$	3.347 97 (41)

TABLE 1.2: numerical values for the sixth order A_i coefficients [33]

QED terms of order higher than three are not known. So the total QED contribution to a_τ is [33]

$$a_\tau^{\mathrm{QED}} = 117\,324\,(2)\ \cdot\ 10^{-8} \tag{1.18}$$

The error $\delta a_\tau^{\mathrm{QED}}$ is the uncertainty $\delta C_\tau^{(8)}(\alpha/\pi)^4 \sim \pi^2\ln^2(m_\tau/m_e)(\alpha/\pi)^4 \sim 2\cdot 10^{-8}$ that the author in Ref. [33] assigned to a_τ^{QED} for the uncalculated four-loop contributions. Compared to this one, the errors due to the uncertainties of the $O(\alpha^2)$ and $O(\alpha^3)$ terms are negligible.

1.3.2 Electroweak contribution

With respect to the QED one-loop term, the electroweak correction to a_τ is suppressed by the ratio $(m_\tau/M_W)^2 \approx 4.8\cdot 10^{-4}$, where $M_W = 80.399(23)$ GeV is the mass of the

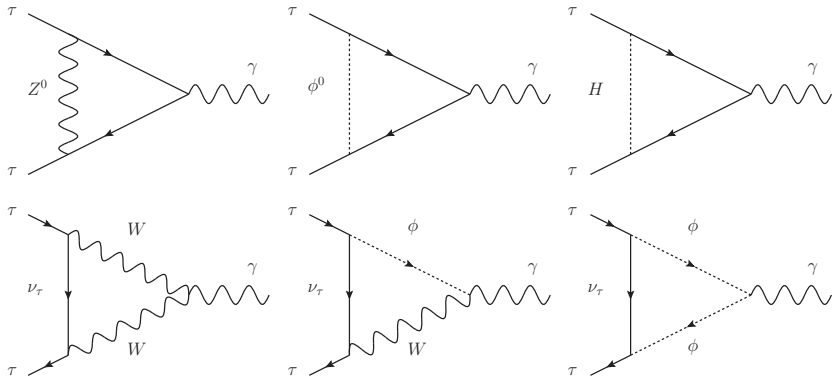

FIGURE 1.3: The one-loop electroweak contributions to a_τ. The diagram with a W and a Goldstone boson ϕ must be counted twice.

W boson [35]. The EW contribution is therefore of the same order of magnitude as the three-loop QED one. The one-loop diagrams involved are shown in Fig. 1.3.

The analytic expression for the one-loop EW contribution to a_τ reads [36–40]

$$a_\tau^{\mathrm{EW}}(\text{one-loop}) = \frac{5G_F m_\tau^2}{24\sqrt{2}\pi^2}\left[1+\frac{1}{5}(1-4\sin^2\theta_W)^2 + O\left(\frac{m_\tau^2}{M_{Z,W,H}^2}\right)\right], \tag{1.19}$$

where $G_F = 1.6637(1)\cdot 10^{-5}\mathrm{GeV}^{-2}$ is the Fermi coupling constant [35], M_Z, M_W, M_H are the masses of the Z, W and Higgs bosons, and $\sin^2\theta_W(M_Z) = 0.231\,22\,(15)$ is the Weinberg angle [35]. From the last equation we get [18]

$$a_\tau^{\mathrm{EW}}(\text{one-loop}) = 55.2\,(1)\cdot 10^{-8}. \tag{1.20}$$

The two-loop correction to a_τ^{EW} involves 1678 diagrams [41, 42]. Naively one would expect the two-loop EW terms to be of order $(\alpha/\pi)\cdot a_\tau^{\mathrm{EW}}$ and thus negligible, on the contrary they contribute quite substantially because of the appearance of terms enhanced by a factor of $\log(M_{W,Z}/m_f)$, where m_f is a fermion mass scale much smaller than M_W. The two-loop EW contribution is [18, 42]

$$a_\tau^{\mathrm{EW}}(\text{two-loop}) = -7.74\cdot 10^{-8}, \tag{1.21}$$

a 14% reduction of the one-loop result. The three-loop EW corrections to a_τ were determined to be extremely small via renormalization-group analysis [43]. The total EW part is [18]

$$a_\tau^{\mathrm{EW}} = 47.4\,(5)\cdot 10^{-8}. \tag{1.22}$$

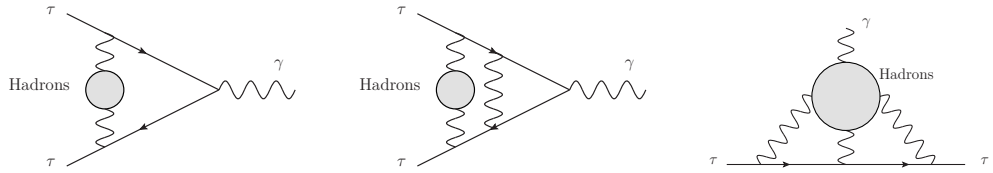

(A) Leading order correction (B) A higher order correction (C) Light-by-light

FIGURE 1.4: Examples of hadronic contributions to a_τ.

1.3.3 The Hadronic Contribution

Unlike the QED part, the contribution from quantum fluctuations involving hadrons cannot be computed from theory alone, because most of the hadronic physics occurs in the low-energy non-perturbative QCD regime. At the leading-order (α^2) the corresponding Feynman diagram is shown in Fig. 1.4, which involves one hadronic insertion. By virtue of the analyticity structure of the vacuum polarization correlator, the hadronic contribution to the magnetic anomaly can be calculated via the dispersion integral [44–47]:

$$a_\tau^{\mathrm{HLO}} = \frac{m_\tau^2}{12\pi^3}\int_{4m_\pi^2}^{\infty} ds \frac{\sigma^{(0)}(e^+e^- \to \text{hadrons})K_\tau(s)}{s}, \tag{1.23}$$

where $\sigma^{(0)}(e^+e^- \to \text{hadrons})$ is the total hadronic cross section of the e^+e^- annihilation in the Born approximation, and $K_\tau(s)$ is a bounded function of the energy monotonously increasing to unity at $s \to \infty$ [44–47]:

$$K_\tau(s) = \int_0^1 dy \frac{y^2(1-y)}{y^2 + s(1-y)/m_\tau^2}. \tag{1.24}$$

The computation gives [18]

$$a_\tau^{\mathrm{HLO}} = 337.5\,(3.7)\cdot 10^{-8}. \tag{1.25}$$

As for the QED three-loop case, the hadronic higher-order contribution (α^3) can be divided into two parts: $a_\tau^{\mathrm{HHO}} = a_\tau^{\mathrm{HHO}}(\mathrm{vp}) + \mathrm{a}_\tau^{\mathrm{HHO}}(\mathrm{lbl})$. The first one arises from diagrams containing hadronic self-energy insertions in the photon propagators and can be estimated as in the leading-order case. The second term is the hadronic light-by-light contribution and cannot be directly determined via a dispersion relation approach. Its evaluation therefore relies on specific models of low-energy hadronic interactions with electromagnetic currents. The latest estimates are $a_\tau^{\mathrm{HHO}}(\mathrm{vp}) = 7.6\,(2)\cdot 10^{-8}$ [48] and $a_\tau^{\mathrm{HHO}}(\mathrm{lbl}) = 5\,(3)\cdot 10^{-8}$ [18]. The total hadronic contribution is [18]

$$a_\tau^{\mathrm{HAD}} = a_\tau^{\mathrm{HLO}} + a_\tau^{\mathrm{HHO}}(\mathrm{vp}) + \mathrm{a}_\tau^{\mathrm{HHO}}(\mathrm{lbl}) = 350.1(4.8)\cdot 10^{-8}. \tag{1.26}$$

Now we can add up all the discussed terms to derive the SM prediction to a_τ:

$$a_\tau^{\mathrm{SM}} = a_\tau^{\mathrm{QED}} + a_\tau^{\mathrm{EW}} + a_\tau^{\mathrm{HAD}}, \tag{1.27}$$

where

$$a_\tau^{\mathrm{QED}} = 117\,324\,(2) \cdot 10^{-8}, \tag{1.28}$$

$$a_\tau^{\mathrm{EW}} = 47.4\,(5) \cdot 10^{-8}, \tag{1.29}$$

$$a_\tau^{\mathrm{HAD}} = 350.1(4.8) \cdot 10^{-8}. \tag{1.30}$$

The final results is

$$a_\tau^{\mathrm{SM}} = 117\,721\,(5) \cdot 10^{-8}. \tag{1.31}$$

Quite generally, New Physics associated with a scale Λ is expected to modify the SM prediction of the anomalous magnetic moment of a lepton l of mass m_l by a contribution of order $a_l^{\mathrm{NP}} \sim m_l^2/\Lambda^2$. Therefore, given the large factor $(m_\tau/m_\mu)^2 \sim 283$, the $g-2$ of the tau is much more sensitive than the one of the muon to EW and NP effects which give contribution $\sim m_l^2$, making its measurement an excellent opportunity to unveil or constrain NP effects.

Another interesting feature can be observed comparing the magnitude of EW and hadronic contributions to the muon and tau lepton $g-2$. The EW contribution to the tau magnetic moment is only a factor 7 smaller than the hadronic one, compared to a factor 45 in the case of the muon. Also, while the EW contribution to a_μ^{SM} is only a factor of 3 larger than the present uncertainty of the hadronic contribution, this factor raises to 10 for the τ lepton. If an NP contribution were of the same order of magnitude as that of the EW, from a purely theoretical point of view, the $g-2$ of the tau would provide a much cleaner test of the presence (or absence) of such NP effects than the muon one. Indeed, if this were the case, such an NP contribution to the tau lepton anomalous magnetic moment could be much larger than the hadronic uncertainty, which is currently the limiting factor of the SM prediction.

1.4 The tau lepton EDM

As previously discussed, the EDM interaction violates discrete CP symmetry. In the SM, with massless neutrinos, the only source of CP violation is the CKM-phase (and a possible θ-term in QCD sector). Therefore, a fundamental lepton EDM arises from virtual quarks linked to the lepton through virtual $W^\pm$. It can be shown [49, 50] that all CP-violating amplitudes are proportional to the Jarlskog invariant J defined via the

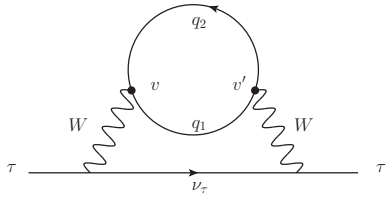

FIGURE 1.5: This two-loop diagrams does not contribute to lepton EDM. The external photon (not shown) can be attached to any charged particle

convention-invariant equation [50]

$$\mathrm{Im}\left[V_{ij}V_{kl}V_{il}^{*}V_{kj}^{*}\right] = J\sum_{m,n}\varepsilon_{ikm}\varepsilon_{jln}. \tag{1.32}$$

Using the convention for the CKM matrix in [51], it can be written as

$$J = s_{12}\, s_{13}\, s_{23}\, c_{12}\, c_{13}^{2}\, c_{23}\, \sin(\delta), \tag{1.33}$$

where $s_{ij} = \sin\theta_{ij}$ and $c_{ij} = \cos\theta_{ij}$, θ_{ij} are the three mixing angles of the matrix V_{CKM}, and δ is the KM phase responsible for all CP-violating phenomena in flavor-changing processes in the SM [52]. Hence, loop diagrams can contribute to a lepton (or quark) EDM if they are sensitive to the imaginary part of the V_{CKM} matrix elements.

Naively one may expect a contribution to lepton EDMs from the two-loop diagram of Fig. 1.5. However, for each CKM matrix contribution V_{ij} at one vertex v, there is an other V_{ij}^{*} at the other vertex v'. Hence, the overall amplitude cannot contain a CP-violating phase. Then, one can consider three-loop diagrams. The situation was first analyzed in some detail in [53], but it was subsequently shown that the various terms from three-loop diagrams cancel [54] (see Fig. 1.6), yielding a net contribution of zero in the absence of gluonic corrections to the quark lines.

For this reason, lepton EDMs in the SM are predicted to be extremely small, of the $\mathcal{O}(10^{-38} - 10^{-35})\, e{\cdot}\mathrm{cm}$ [55], which is far below the current experimental capabilities. In fact, the current experiments can only probe $d_\tau \sim \mathcal{O}(10^{-17})\, e{\cdot}\mathrm{cm}$, but also for the electron the situation is similar: $d_e^{\mathrm{exp}} < 10.5\times10^{-28} e{\cdot}$ cm [56] when $d_e^{\mathrm{SM}} \sim \mathcal{O}(10^{-38})\, e{\cdot}\mathrm{cm}$. It is hard to imagine improvements in sensitivity by more than ten orders of magnitude. However, new EDM effects could arise at one or two loop from NP that violate P and T, and be much larger than the tiny SM prediction even if they come from high mass scales. They generally induce large contributions to lepton and neutron EDMs [57], and although there has been no experimental evidence for an EDM so far, there is considerable hope to gain new insights into the nature of CP violation through this kind of experiments.

The current 95% confidence level limits on the EDM of the tau lepton are

$$\begin{aligned} &-2.2 < \mathrm{Re}(d_\tau) < 4.5 \ \ (10^{-17}\, e\,\mathrm{cm}), \\ &-2.5 < \mathrm{Im}(d_\tau) < 0.8 \ \ (10^{-17}\, e\,\mathrm{cm}); \end{aligned} \tag{1.34}$$

they were obtained by the Belle collaboration [19] following the analysis of Ref. [58] for the impact of an effective operator for the tau EDM in the process $e^+e^- \to \tau^+\tau^-$.

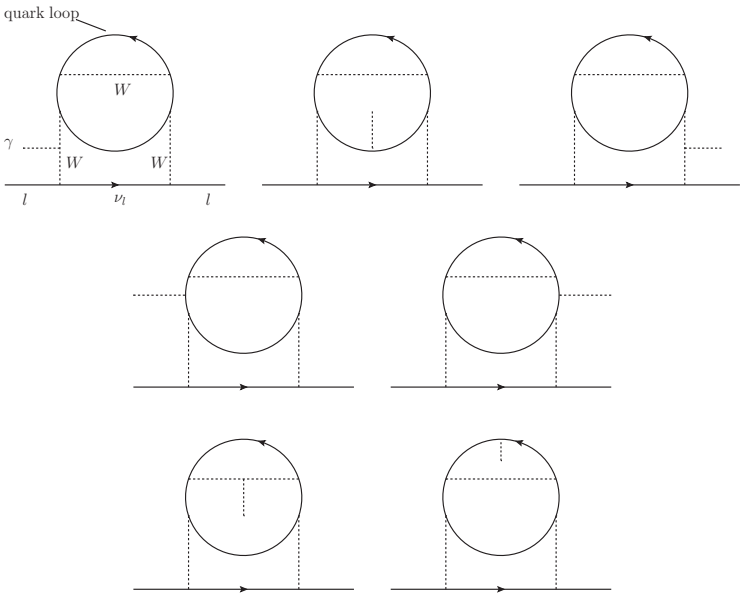

FIGURE 1.6: The sum of contributions to the tau EDM from these three-loop diagrams vanishes in the SM as shown in Ref. [54]. For clarity here the vector boson propagators are drawn with dashed lines.

1.5 Experimental determination of a_τ

The present resolution on the tau anomalous magnetic moment is only of $\mathcal{O}(10^{-2})$ [17], more than an order of magnitude larger than its SM prediction in Eq. (1.31). In fact, while the SM value of a_τ is known with a tiny uncertainty of 5×10^{-8}, the tau short lifetime has so far prevented the determination of a_τ by measuring the tau spin precession in a magnetic field, like in the electron and muon $g-2$ experiments. The current PDG limit on the tau $g-2$ was derived in 2004 by the DELPHI collaboration from $e^+e^- \to e^+e^-\tau^+\tau^-$ total cross section measurements at $\sqrt{s}$ between 183 and 208 GeV at LEP2 (the study of a_τ via this channel was proposed in [59]). The measured values of the cross-sections were used to extract limits on the tau $g-2$ by comparing them to the SM values, assuming that possible deviation were due to non-SM values of a_τ. The 95% CL

limit obtained is [17]

$$-0.052 < a_\tau < 0.013, \tag{1.35}$$

that can be also expressed in the form of central value and error as [17]

$$a_\tau = -0.018\,(17). \tag{1.36}$$

In [60] the reanalysis of various measurements, the $e^+e^- \to \tau^+\tau^-$ cross section, the transverse τ polarization and asymmetry at LEP and SLD, as well as the decay width $\Gamma(W \to \tau\nu_\tau)$ at LEP and Tevatron allowed the authors to set a model-independent limit on NP contributions,

$$-0.007 < a_\tau^{\rm NP} < 0.005, \tag{1.37}$$

a bound stronger than that in Eq. (1.35). This analysis, like earlier ones, was performed without radiative corrections, but the authors checked that the inclusion of initial-state radiation did not affect significantly the obtained bounds. However this analysis is not taken into account by the PDG data group because in [60] it is assumed $\mathrm{Im}(a_\tau) = 0$.

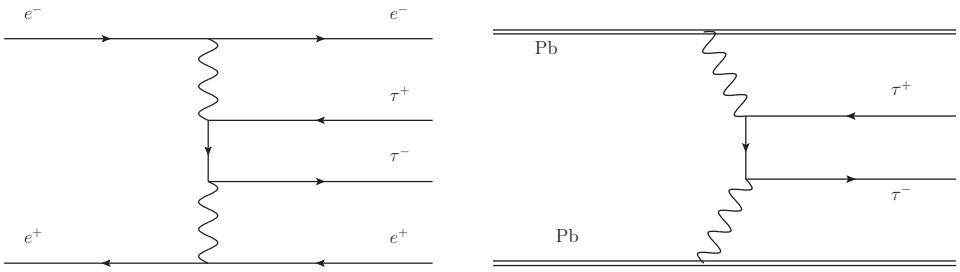

FIGURE 1.7: Current bound on a_τ was derived from $e^+e^- \to e^+e^-\tau^+\tau^-$ by the DELPHI collaboration [17] (left).
It was suggested to search for a_τ at LHC in heavy ions collision [61] (right)

In [62] it was suggested to study the radiative decay $W \to \tau\bar{\nu}_\tau\gamma$ as a function of the anomalous magnetic moment of the tau. Authors computed the future statistical bounds achievable at Tevatron and LHC (1 year run) through the study of the normalized differential decay rate for $W \to \tau\bar{\nu}_\tau\gamma$ ($\frac{d\Gamma}{dE_\gamma}/\Gamma_{\rm SM}$). The expected sensitivity at Tevatron and LHC (1 year run) are, respectively, 2.3×10^{-2} and 2.5×10^{-3} at 90% CL (but no background is considered in this analysis).

In [61] it was investigated the possibility of using heavy-ion collision at the LHC for measuring the electromagnetic properties of tau lepton. The proposed process,

$$\mathrm{PbPb} \to \mathrm{PbPb}\,\gamma\gamma \to \mathrm{PbPb}\,\tau\tau, \tag{1.38}$$

has the advantage that the photons can be considered as initial partons and therefore they are almost real ($q^2 \sim 0$). However, in this case, the longitudinal momentum of the $\tau^+\tau^-$ pair cannot be reconstructed. The expected 1σ bounds at the LHC, for the analyzed subchannel $\gamma\gamma \to \tau\tau \to \ell\rho\nu\nu\nu$, is $|a_\tau| < 3 \times 10^{-3}$ [61].

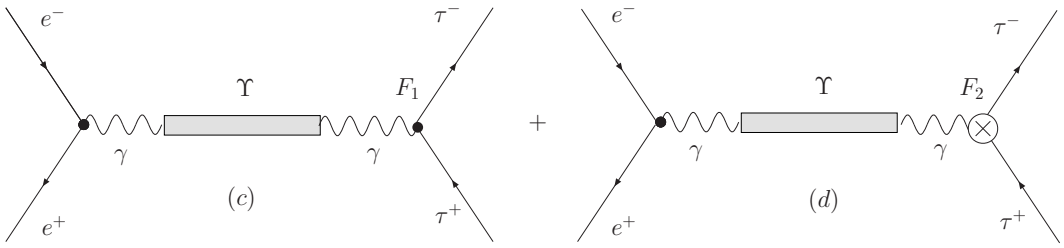

FIGURE 1.8: In Ref. [16] was suggested to measure $F_{2V}(M_\Upsilon^2)$ in $e^+e^- \to \Upsilon \to \tau^+\tau^-$. Diagrams: (c) Υ production, (d) F_{2V} in Υ production.

Yet another method would use the channeling of polarized taus in a bent crystal similarly to the suggestion for the measurement of magnetic moments of short-living baryons [63]. In these kind of experiments, a strong electric field is applied to the bent crystal and properly tuned so that the electric field is seen by the fast-moving particle as a large mega-tesla magnetic field: the spin then precesses significantly before the particle decay, and it can be later measured from the angular distribution of the final state particles. This method has been successfully tested by the E761 collaboration at Fermilab, which measured the magnetic moment of the Σ^+ hyperon [64]. The challenge of this method is to produce a polarized beam of taus. In the case of muon $g-2$ experiment, the polarized muons come from pions that almost totally decay $\pi^+ \to \mu^+\nu_\mu$. In the case of the tau lepton, one could use the decay $B^+ \to \tau^+\nu_\tau$, which would produce polarized tau leptons [65], however this particular decay of the B has a very tiny branching ratio of $\mathcal{O}(10^{-4})$. In 1991, when this proposal was published, the idea seemed completely unlikely. Nonetheless, in the era of B factories, when the decay $B^+ \to \tau^+\nu_\tau$ is already observed by the Belle collaboration [66], the realization of this idea in a dedicated experiment is definitively not excluded.

The future high-luminosity B factory Belle-II [67] offers also new opportunities to improve the determination of tau electromagnetic properties. Authors in [16] proposed to determine the Pauli form factor $F_{2V}(q^2)$ of the tau via $\tau^+\tau^-$ production in e^+e^- collisions at the Υ resonances (Υ(1S), Υ(2S) and Υ(3S)) with a sensitivity of $\mathcal{O}(10^{-5})$ or even better. In super B factories the center-of-mass energy is $\sqrt{s} \sim M_{\Upsilon(4S)} = 10$ GeV, and therefore $F_{2V}(q^2)$ is no longer the magnetic anomaly. When attempting to extract the value of F_{2V} from scattering experiments (as opposed to using a background magnetic field) one encounters additional complications due to the contributions of various other Feynman graphs, not related to the magnetic form factor.

In particular in $e^+e^- \to \tau^+\tau^-$ there are contributions not only from the usual s-channel one-loop vertex corrections but also from box diagrams that, by the way, are gauge dependent. The contributions of the latter may interfere in the experimental determination of what we call $F_{2V}(q^2)$, i.e. the magnetic part coming only from the vertex, and should be somehow subtracted out. This may be done either by computing the box contributions and subtracting them from the cross section, or by performing the measurement in a kinematic region where the boxes happen to be numerically subleading. Indeed, the strategy proposed in [16] for eliminating the contamination from the boxes is to measure the observables on top of the Υ resonances: in this kinematic regime the (non-resonant) box diagrams are numerically negligible, and only one loop corrections to the $\gamma\tau\tau$ vertex are relevant (Fig. 1.8).

However, at Belle II it is difficult to resolve the narrow peaks of the $\Upsilon(1S, 2S, 3S)$ in the $\tau^+\tau^-$ decay channel (the $\Upsilon(4S)$ decays almost entirely in $B\bar{B}$) because of the natural irreducible beam energy spread associated to any e^+e^- synchrotron. Indeed, the total visible cross section of these resonances is not a perfect Breit-Wigner, but actually the convolution of the theoretical Breit-Wigner cross section with a gaussian spread,

$$\sigma_{\text{vis.}} = \int \sigma(s) \frac{1}{\sqrt{2\pi}\sigma_\varepsilon} \exp\left[-\frac{(\sqrt{s} - M_\Upsilon)^2}{2\sigma_\varepsilon^2}\right] d\sqrt{s}, \tag{1.39}$$

where $\sigma_\varepsilon \sim 3.3$ MeV [68] is the irreducible beam energy spread of the Super-KEKB accelerator at $\sqrt{s} = M_\Upsilon$, and $\sigma(s)$ is the total cross section in the Breit-Wigner approximation:

$$\begin{aligned} \sigma_{ee\to\Upsilon\to\tau\tau}(s) &= 12\pi \frac{\text{Br}(\Upsilon \to ee)\text{Br}(\Upsilon \to \tau\tau)\Gamma_{\text{tot}}^2}{(s - M_\Upsilon^2)^2 + M_\Upsilon^2\Gamma_{\text{tot}}^2} \\ &= \sigma_{\text{peak}} \frac{M_\Upsilon^2\Gamma_{\text{tot}}^2}{(s - M_\Upsilon^2)^2 + M_\Upsilon^2\Gamma_{\text{tot}}^2}, \end{aligned} \tag{1.40}$$

that can be approximated in the limit of narrow resonance, $\sigma_\varepsilon \gg \Gamma_{\text{tot}}$, as

$$\sigma_{ee\to\Upsilon\to\tau\tau}(s) = \sigma_{\text{peak}} \pi M_\Upsilon \Gamma_{\text{tot}} \delta(s - M_\Upsilon^2). \tag{1.41}$$

Here we have defined the cross section at peak $\sigma_{\text{peak}} = 12\pi\text{Br}(\Upsilon \to ee)\text{Br}(\Upsilon \to \tau\tau)/M_\Upsilon^2$. The expression for the maximum visible cross section, obtained substituting Eq. (1.40) into Eq. (1.39), is

$$\sigma_{\text{vis.}}^{\text{max}} = x\,\sigma_{\text{peak}}, \quad \text{with } x = \sqrt{\frac{\pi}{8}}\frac{\Gamma_{\text{tot}}}{\sigma_W}. \tag{1.42}$$

In Tab. 1.3 we compare the visible resonant cross sections for $e^+e^- \to \Upsilon \to \tau^+\tau^-$ to the non-resonant cross section at $\sqrt{s} = M_\Upsilon$: $\sigma_{\text{non-res.}} = 4\pi\alpha^2/(3s) + \mathcal{O}(\alpha^3) = 0.92$ nb [69]. The situation at Belle was pretty similar, indeed the energy spread at KEKB was $\sigma_\varepsilon \sim$

Υ	M_Υ [GeV]	Γ_{tot} [keV]	σ_{peak} [nb]	x	$\frac{\sigma_{\text{vis}}^{\text{max}}}{\sigma_{\text{non-res.}}}$
$\Upsilon(1S)$	9.46	54	101	1.0×10^{-3}	106%
$\Upsilon(2S)$	10.02	31	56	6.0×10^{-3}	36%
$\Upsilon(3S)$	10.35	20	63	3.8×10^{-3}	26%
$\Upsilon(4S)$	10.58	20×10^3	-	-	-

TABLE 1.3: Estimated visible cross section at Belle II for $e^+e^- \to \Upsilon \to \tau^+\tau^-$. The adopted machine parameters are those in Ref. [68].

3.2 MeV [70]. At the Belle II experiment the $\tau^+\tau^-$ events produced with beams at a centre of mass energy $\sqrt{s} \sim M_\Upsilon$ are mostly due to non-resonant interaction, indeed the visible resonant cross sections are of the same order of the non-resonant ones or even smaller. Even for the multihadron events in the region of $\Upsilon(1S, 2S, 3S)$, the non-resonant cross section dominates with respect to the resonant one (see for example [71]).

1.6 Radiative leptonic τ decays

We propose to measure the dipole moments of the tau lepton through its radiative leptonic decays:

$$\tau^- \to l^- \nu_\tau \bar{\nu}_l \gamma, \quad \text{with } l = e, \mu. \tag{1.43}$$

The possibility to set bounds on a_τ via the radiative leptonic τ decays was suggested long ago in [72]. In that article the authors proposed to take advantage of a radiation zero of the LO differential decay rate which occurs when, in the tau rest frame, the final lepton l and the photon are back-to-back, and l has maximal energy. Since a non-standard contribution to a_τ spoils this radiation zero, precise measurements of this phase-space region could be used to set bounds on its value. However, this method is only sensitive to large values of a_τ (at the radiation zero the dependence on non-standard a_τ contributions is quadratic), and preliminary studies with Belle data show no significant improvement of the existing limits (see Sec. 1.11).

The authors of Ref. [60] and [58] applied effective Lagrangian techniques to study a_τ and d_τ. Our strategy is similar: the energy scale $\sqrt{s} \sim m_\tau$ involved in tau radiative decays allow us to study the tau dipole moments introducing, beside the SM Lagrangian, two new effective terms of the form:

$$\mathcal{L}_{\text{eff}} = \mathcal{L}_{\text{SM}} + c_a \frac{e}{4\Lambda} \mathcal{O}_a - c_d \frac{i}{2\Lambda} \mathcal{O}_d, \tag{1.44}$$

where the operators $\mathcal{O}_{a,d}$ are given by

$$\begin{aligned} \mathcal{O}_a &= \bar{\tau}\sigma_{\mu\nu}\tau\, F^{\mu\nu}, \\ \mathcal{O}_d &= \bar{\tau}\sigma_{\mu\nu}\gamma_5\tau\, F^{\mu\nu}. \end{aligned} \tag{1.45}$$

The scale Λ represents the scale where any kind of physics which is not described by $\mathcal{L}_{\rm SM}$ generates a contribution to the tau's electric or magnetic dipole moment and is therefore larger at least than the electroweak scale, i.e. $\Lambda > M_Z$. For simplicity we assume the scale Λ to be equal for both operators $\mathcal{O}_{a,d}$, knowing that actually the scale for the EDM is much higher than that for the $g-2$. The contributions from the two effective operators $\mathcal{O}_{a,d}$ to the electromagnetic form factors are the same for $q^2 = 0$ as for $q^2 \neq 0$. The point is that only higher dimensional operators would give rise to a difference between these two cases, which means that such contributions are suppressed by higher powers of q^2/Λ^2 [60]. In our case, q^2 may be of the order of m_τ^2 while Λ is certainly higher than M_Z and we may therefore safely neglect contributions from higher dimensional operators. Of course, the requirement that $q^2 \ll \Lambda^2$ is the fundamental hypothesis of our effective Lagrangian approach.

Even if the set of two operators introduced in Eqs. (1.44) and (1.45) are not gauge invariant under the gauge group $SU(2)_L \times U(1)_Y$, they can be recovered from dimension-six gauge invariant operators,

$$\mathcal{O}_B = \frac{C_{eB\varphi}^{33}}{2\Lambda^2}\left(\bar{\ell}_{\rm L}\sigma^{\mu\nu}\tau_{\rm R}\right)\varphi B_{\mu\nu} + \text{h.c.}\,, \tag{1.46}$$

$$\mathcal{O}_W = \frac{C_{eW}^{33}}{2\Lambda^2}\left(\bar{\ell}_{\rm L}\sigma^{\mu\nu}\tau_{\rm R}\right)T^a\varphi\, W_{\mu\nu}^a + \text{h.c.}\,, \tag{1.47}$$

after spontaneous symmetry breaking [60, 73–75]. Here $\ell_{\rm L} = (\nu_{\tau{\rm L}}, \tau_{\rm L})$ is the tau leptonic doublet, φ is the Higgs doublet, $B^{\mu\nu}$ and $W^{\mu\nu}$ the $U(1)_Y$ and $SU(2)_L$ field strength tensors, and T^a the generators of $SU(2)_L$. For our phenomenological study however it is simpler to adopt the Lagrangian in Eq. (1.44).

The effective Lagrangian in (1.44) gives the following predictions for the tau dipole moments:

$$a_\tau = \frac{\alpha}{2\pi} + c_a\frac{m_\tau}{\Lambda} + \cdots \tag{1.48}$$

$$d_\tau = c_d\,\frac{1}{\Lambda} + \cdots \tag{1.49}$$

where the dots indicate higher-order contributions not relevant for our discussion (note, in (1.49), that d_τ has no QED contribution). We then define the parameters

$$\tilde{a}_\tau \equiv c_a \frac{m_\tau}{\Lambda}, \quad \tilde{d}_\tau \equiv c_d \frac{1}{\Lambda}. \tag{1.50}$$

Our goal is to provide a method to determine $\tilde{a}_\tau$ and $\tilde{d}_\tau$ with a precision of $O(10^{-3})$ or better. For this reason, we computed the decay rate prediction for the processes in (1.43) including radiative corrections at next-to-leading order (NLO) in QED and the non-negligible contribution from the W-boson propagator of $\mathcal{O}(m_\tau^2/M_W^2) \sim 5 \cdot 10^{-4}$. The comparison of this NLO prediction, modified by the additional terms in (1.44), to sufficiently precise data allows to determine $\tilde{a}_\tau$ and $\tilde{d}_\tau$ (and thereby a_τ via (1.48)) possibly down to the level of $O(10^{-4})$.

1.7 Muon Decay and the definition of G_F

Before discussing tau leptonic radiative decays, it is worthwhile to recall the relation between muon decay and the definition of the Fermi constant G_F.* Let us focus our attention on muon decay. In the SM, the full inclusive decay rate of

$$\mu^- \to e^- \, \nu_\mu \, \bar{\nu}_e(\gamma) \tag{1.51}$$

is [77]

$$\Gamma_{(\mu)} = \frac{G_\mu^2 M^5}{192\pi^3} F\big(r^2\big) \, (1 + \delta_\mu) \, [1 + \delta_{\rm W}(M, m)] \,, \tag{1.52}$$

where $r = m/M$, $r_{\rm W} = M/M_{\rm W}$,

$$F(t) = 1 - 8t + 8t^3 - t^4 - 12t^2 \ln t \tag{1.53}$$

is a phase-space factor and M and m are, respectively, the muon and electron mass. Also,

$$\frac{G_\mu}{\sqrt{2}} \equiv \frac{g^2}{8M_{\rm W}^2} \, (1 + \Delta r) \,, \tag{1.54}$$

where g is the $\mathrm{SU}(2)_L$ gauge coupling constant and Δr is the electroweak correction introduced by Sirlin in Ref. [78]. The term δ_μ is the QED correction evaluated in the Fermi V–A theory; it includes the corrections of virtual and real photons up to $\mathcal{O}(\alpha^2)$, as well as the tiny contribution of the decay $\mu^- \to e^- \nu_\mu \bar{\nu}_e e^+ e^-$ [79–88]. Moreover,

$$\delta_{\rm W}(M, m) = \frac{3}{5} \, r_{\rm W}^2 \frac{\big(1 - r^2\big)^5}{F(r^2)} + \mathcal{O}\big(r_{\rm W}^4\big) \tag{1.55}$$

*work in collaboration with L. Mercolli and M. Passera [76]

is the tree-level correction induced by the W-boson propagator recently computed by Ferroglia, Greub, Sirlin and Zhang [77]. Its leading and next-to-leading contributions can be immediately derived from (1.55): $(3/5)(M/M_{\rm W})^2$ and $(9/5)(m/M_{\rm W})^2$, respectively. While the leading one is well known in the literature [89, 90], the next-to-leading term differs from that reported in earlier publications [91–93]. We also computed these tree-level correction induced by the W-boson propagator and we confirmed the result in (1.55), in agreement with Ref. [77]. We should add that while $(3/5)(m_\mu/M_{\rm W})^2 \sim 1.0 \times 10^{-6}$ is of the same magnitude as the present experimental relative uncertainty of the muon decay rate in (1.52), 1.0 ppm, the subleading contribution $(9/5)(m_e/M_{\rm W})^2 \sim 7.3 \times 10^{-11}$ is out of experimental reach in the foreseeable future. Moreover, radiative corrections to muon decay of $\mathcal{O}(\alpha^3) \sim 10^{-7}$ and $\mathcal{O}(\alpha\, m_\mu^2/M_{\rm W}^2) \sim 10^{-8}$ have not yet been computed.

The Fermi constant of weak interactions, G_F, is defined from the muon lifetime τ_μ evaluated in the Fermi V–A theory,

$$\mathcal{L} = -\frac{G_F}{\sqrt{2}} \left[\bar{\psi}_{\nu_\mu} \gamma^\alpha \left(1 - \gamma_5\right) \psi_\mu\right] \left[\bar{\psi}_e \gamma_\alpha \left(1 - \gamma_5\right) \psi_{\nu_e}\right] + \text{h.c.}, \tag{1.56}$$

plus QED to leading order in the weak interaction coupling constant. We remind the reader that to leading order in G_F, but to all orders in α, the radiative corrections to muon decay in the Fermi V–A theory are finite after mass and charge renormalization [94]. Specifically, the present Particle Data Group (PDG) definition of G_F is given by the relation [95, 96]

$$\frac{1}{\tau_\mu} = \frac{G_F^2 m_\mu^5}{192\pi^3} F\left(\frac{m_e^2}{m_\mu^2}\right) \left(1 + \delta_\mu\right). \tag{1.57}$$

This definition is independent of $M_{\rm W}$, whereas earlier ones (see, for example, PDG 2010 [35]) included the additional factor $[1 + (3/5) m_\mu^2/M_{\rm W}^2]$ on the r.h.s. of (1.57). Since this factor does not arise in the Fermi theory framework, it is more natural not to include it in the definition in (1.57). Also, identifying (1.57) with (1.52) one finds the relation [77]

$$G_\mu^2 = G_F^2 / \left[1 + \delta_{\rm W}(m_\mu, m_e)\right], \tag{1.58}$$

with $\delta_{\rm W}(m_\mu, m_e) = 1.04 \times 10^{-6}$ given by (1.55).

The muon decay rate in (1.52) can be immediately extended to the tau leptonic decays

$$\tau^- \to l^- \nu_\tau \bar{\nu}_l \left(\gamma\right) \quad \text{with } l = e, \mu, \tag{1.59}$$

identifying M with m_τ and m with m_e or m_μ. The QED correction δ_μ should also be replaced by δ_τ, the appropriate one for these decays, while the electroweak corrections are the same as those contained in G_μ for muon decay [97]. Furthermore, in order to express these tau decay rates in terms of G_F, one should also replace G_μ in (1.52)

via (1.58), thus obtaining

$$\Gamma_{(\tau)} = \frac{G_F^2 M^5}{192\pi^3} F\big(r^2\big)\,(1+\delta_\tau)\left[\frac{1+\delta_{\rm W}(M,m)}{1+\delta_{\rm W}(m_\mu,m_e)}\right]. \tag{1.60}$$

Note that the leading contribution to $\delta_{\rm W}(M,m)$, appearing in the numerator in square brackets, is independent of the flavor of the final lepton; it amounts to $(3/5)(m_\tau/M_{\rm W})^2 \sim 2.9\times10^{-4}$. The term $\delta_{\rm W}(m_\mu,m_e)$ in the denominator, due to the relation between G_μ and G_F, has been kept for completeness, but it is of the same order of magnitude as the uncomputed radiative corrections of $\mathcal{O}(\alpha\, m_\tau^2/M_{\rm W}^2) \sim 10^{-6}$. The hadronic corrections to (1.60) are still missing too; they are of $\mathcal{O}(\alpha^2/\pi^2) \sim 10^{-5}$ [85, 98].

Our prediction for the energy-angle distribution of the final charged lepton in the decays (1.51) and (1.59) of a polarized μ^- or τ^- at rest is

$$\begin{aligned}\frac{d^2\Gamma_{(\mu,\tau)}}{dx\, d\cos\theta_l} = \frac{G_F^2 M^5}{192\pi^3}\frac{x\beta}{1+\delta_{\rm W}(m_\mu,m_e)}\times\\ \big\{3x-2x^2+r^2(3x-4)+f(x)\\ +r_{\rm W}^2\big[2x^2-x^3-2r^2\big(1+x-x^2+r^2\big)\big]\\ -\cos\theta_l\; x\beta\,\big[2x-1-3r^2+g(x)\\ +r_{\rm W}^2\,x\,\big(x-2r^2\big)\big]+\mathcal{O}\big(r_{\rm W}^4\big)\big\}\,,\end{aligned} \tag{1.61}$$

where $\beta \equiv |\vec{p}_l|/E_l = \sqrt{1-4r^2/x^2}$, $p_l = (E_l,\vec{p}_l)$ is the four-momentum of the final charged lepton, $x = 2E_l/M$ varies between $2r$ and $1+r^2$, p and $n = (0,\hat{n})$ are the four-momentum and polarization vector of the initial muon or tau, with $n^2 = -1$ and $n\cdot p = 0$, and $\cos\theta_l$ is the angle between $\hat{n}$ and $\vec{p}_l$. The corresponding formula for the decay of a polarized μ^+ or τ^+ is simply obtained inverting the sign in front of $\cos\theta_l$ in (1.61).

The functions $f(x)$ and $g(x)$ are the QED radiative corrections; $f(x)$, contributing to the isotropic (θ_l-independent) part, has been calculated up to $\mathcal{O}(\alpha^2)$, while $g(x)$, contributing to the anisotropic one, is known up to leading $\mathcal{O}(\alpha^2)$ effects [79–82, 99–104]. The hadronic corrections to (1.61), which are of $\mathcal{O}(\alpha^2/\pi^2)$, were computed for the decay of the muon, but not yet for the tau [105]. The terms proportional to $r_{\rm W}^2$ are induced by the W-boson propagator. The leading ones, of $\mathcal{O}(r_{\rm W}^2)$, agree with those of Ref. [106]. To our knowledge, the calculation of the subleading terms, of $\mathcal{O}(r^2 r_{\rm W}^2)$, has first been presented in our article [76].

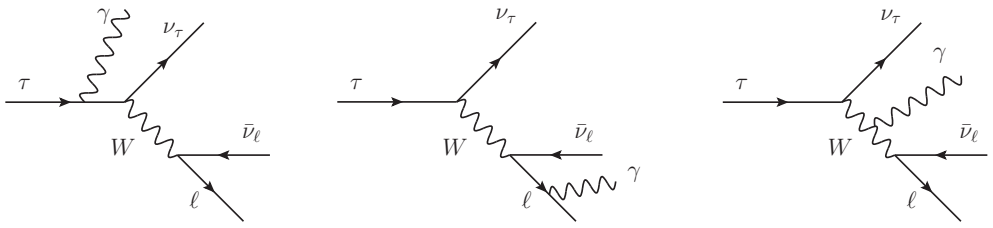

FIGURE 1.9: tau leptonic radiative decays, the SM amplitudes in the unitary gauge.

1.8 Radiative tau decays: LO contributions

We can now turn our attention to the decays

$$\tau^- \to l^- \bar{\nu}_l \nu_\tau \gamma, \quad \text{with } l = e, \mu, \tag{1.62}$$

where the photon is detected and measured. The SM leading-order (LO) prediction for the differential decay rate in Eq. (1.62) of a polarized τ^- is, in the tau lepton rest frame,

$$\frac{d^6\Gamma^{\rm LO}}{dx\, dy\, d\Omega_l\, d\Omega_\gamma} = \frac{\alpha G_F^2 m_\tau^5}{(4\pi)^6} \frac{x\beta}{1+\delta_{\rm W}(m_\mu, m_e)} \times \Big[G(x,y,c) + x\,\beta\,\hat{n}\cdot\hat{p}_l\, J(x,y,c) \; + y\,\hat{n}\cdot\hat{p}_\gamma\, K(x,y,c) \Big], \tag{1.63}$$

where $G_F = 1.166\,378\,7(6) \times 10^{-5}$ GeV^{-2} [107] is the Fermi coupling constant, $\alpha = 1/137.035\,999\,174\,(35)$ [108] is the fine-structure constant, $m_\tau = 1.776\,82\,(16)$ GeV [95] and $r = m_l/m_\tau$. Also $x = 2E_l/m_\tau$ and $y = 2E_\gamma/m_\tau$, where E_l and E_γ are the energy of l and photon. The final charged lepton and photon are emitted at solid angles Ω_l and Ω_γ, respectively, with normalized three-momenta $\hat{p}_l$ and $\hat{p}_\gamma$, and $c \equiv \cos\theta$ is the cosine of the angle between $\hat{p}_l$ and $\hat{p}_\gamma$. The corresponding formula for the radiative decay of a polarized τ^+ (or μ^+) is simply obtained inverting the signs in front of the scalar products $\hat{n}\cdot\hat{p}_l$ and $\hat{n}\cdot\hat{p}_\gamma$ in (1.63).

The function G, and analogously J and K, is given by

$$G(x,y,c) = \frac{4}{3yz^2}\Big[g_{\rm LO}(x,y,z) \; + \; r_{\rm W}^2\, g_{\rm W}(x,y,z) + \mathcal{O}\left(r_{\rm W}^4\right) \Big], \tag{1.64}$$

where $z = xy\,(1-c\beta)\,/2$. The functions $g_{\rm LO}$, $j_{\rm LO}$, and $k_{\rm LO}$, already computed in [81, 90, 109, 110], arise from the pure Fermi V–A interaction, whereas $g_{\rm W}$, $j_{\rm W}$, and $k_{\rm W}$ are the new leading contributions of the W-boson propagator that we obtained in [76]. Their explicit expressions are reported in the appendix.

The operators $\mathcal{O}_a$ and $\mathcal{O}_d$ in Eq. (1.44) generate additional contributions to the differential decay rate in (1.63). They can be summarised in the shift

$$G(x,y,c) \;\to\; G(x,y,c) \;+\; \mathrm{Re}(\tilde{a}_\tau)\, G_a(x,y,c) \;+\; m_\tau\, \mathrm{Im}(\tilde{d}_\tau)\, G_d(x,y,c), \tag{1.65}$$

and similarly for J and K. Moreover, inside the squared bracket of Eq. (1.63) it appears the additional term

$$y\, x\, \beta\, \vec{n}\cdot(\hat{p}_l \times \hat{p}_\gamma)\, \Big[m_\tau\, \mathrm{Re}(\tilde{d}_\tau)\, L_d(x,y,c) + \mathrm{Im}(\tilde{a}_\tau)\, L_a(x,y,c) \Big]. \tag{1.66}$$

All the new contributions induced by effective operators are reported in the appendix. Tiny terms of $O(\tilde{a}^2)$ and $O(\tilde{d}^2)$ were neglected since known to be subleading.

1.9 Radiative tau decays: QED radiative corrections

As shown long ago by Sirlin in [94], to leading order in G_F but to all orders in α, the radiative corrections to muon decay are finite in the Fermi V-A theory. Since this special feature holds also for taus decaying into leptons, we computed all NLO corrections to the processes in (1.62) in the Fermi theory, i.e. collapsing the weak decay, mediated by the W-boson, to an effective four-fermion interaction. This is sufficient for the desired level of precision: pure EW NLO corrections are expected to be of $\mathcal{O}(\alpha\, m_\tau^2/M_W^2)$, which are subleading with respect to the uncomputed two-loop QED of $\mathcal{O}(\alpha^2)$. In this section we present our NLO prediction originated by real photon emission and one-loop virtual photonic corrections. Our results will be also compared with previous works [111, 112] Throughout the calculation, full dependence on the mass ratio $r = m_l/m_\tau$ is taken into account.

1.9.1 Virtual corrections

In the Fermi theory the weak decay mediated by the W boson is collapsed to a four-fermion interaction. Therefore, a virtual photon can be exchanged only between charged fermions, as shown in Fig. 1.10. We performed the computation of one-loop diagrams via Passarino-Veltman reduction of tensor integrals [113], with the use of the *Mathematica* package `FeynCalc` [114] as well as `Form` [115] for the algebra of gamma matrices. We evaluated the analytic expression of the scalar integrals as described in [116] and we numerically checked our expressions with `LoopTools` [117]. We also used the tabulated results in Ref. [118] for box scalar integrals appearing in the amplitudes of Fig. 1.10d. We adopted dimensional regularization, in order to regularize ultraviolet divergences

(UV), and we introduced a fictitious photon mass λ for the treatment of infrared divergences (IR) related to soft photon emission. IR singularities associated to collinear photon emission were already "regularized", since we kept the final charged lepton mass dependence.

UV divergences were removed via on-shell renormalization scheme. After mass and charge renormalization, UV divergences cancel out in the case of tau and muon decay [78], contrary to what happen in general in the Fermi theory. This follows from the fact that, under a Fierz rearrangement that interchanges the wave functions ψ_e and ψ_{ν_μ} in Eq. (1.56), the interaction remains a pure left-handed vector current. This is in sharp contrast to the case of neutron decay in which scalar and pseudo-scalar terms are generated and for which the following argument breaks down. The radiative corrections in that case are not finite.

Indeed once we express the Fermi Lagrangian in term of bare fields,

$$-\frac{G_F}{\sqrt{2}}\bar{\nu}_{0\tau}\left[\gamma^\mu(1-\gamma^5)\right]\tau_0\cdot\bar{l}_0\left[\gamma_\mu(1-\gamma^5)\right]\nu_{0l}+\text{h.c.}\,, \tag{1.67}$$

the wave-function renormalization, $\tau_0=\sqrt{Z_{2\tau}}\tau$ and $l_0=\sqrt{Z_{2l}}l$, leads to

$$-\frac{G_F}{\sqrt{2}}\sqrt{Z_{2\tau}}\sqrt{Z_{2l}}\bar{\nu_\tau}\left[\gamma^\mu(1-\gamma^5)\right]\tau\cdot\bar{l}\left[\gamma_\mu(1-\gamma^5)\right]\nu_l+\text{h.c.}\,. \tag{1.68}$$

As already pointed out in Sec 1.7, G_F is an effective coupling derived from muon decay and does not require the introduction of a bare G_F. By expanding to the first order in α the factor $\sqrt{Z_{2\tau}}\sqrt{Z_{2l}}$,

$$\sqrt{Z_{2\tau}}\sqrt{Z_{2l}}=1+\frac{1}{2}(\delta Z_{2\tau}+\delta Z_{2l})+O(\alpha^2), \tag{1.69}$$

we can identify the second term of the r.h.s. as a sort of "counter term", which exactly cancels the UV divergences in diagrams 1.10b. However, we stress that this cancellation is peculiar and accidental in muon decay and it is not imposed by any renormalization condition, as in the case of charge or mass renormalization.

1.9.2 Real corrections

Emission of a second soft photon with energy below some threshold is experimentally undistinguishable from single emission. If the soft energy-cut satisfies $E_{\min}\ll m_\tau$, then the total amplitude factorizes:

$$\mathcal{M}_{\gamma\gamma}=ie\left[\frac{p_l\cdot\varepsilon'}{p_l\cdot k'}-\frac{p_\tau\cdot\varepsilon'}{p_\tau\cdot k'}\right]\mathcal{M}_\gamma, \tag{1.70}$$

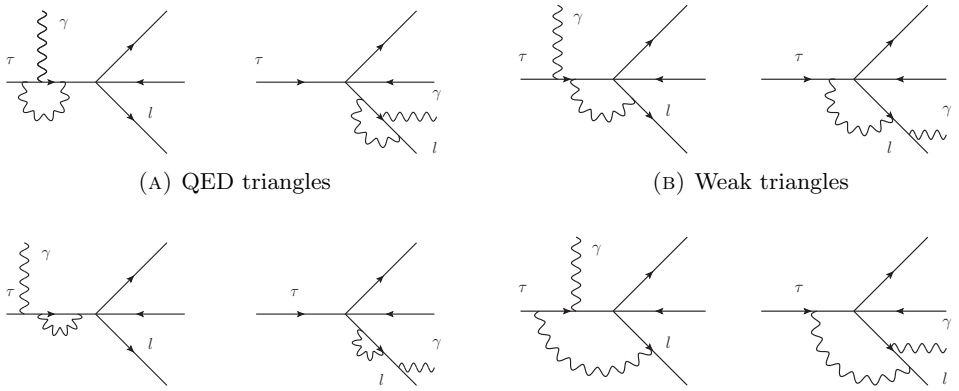

(A) QED triangles (B) Weak triangles

(C) Selfenergies (D) Boxes

FIGURE 1.10: Tau radiative decays: one loop diagrams.

where ε' and k' are the polarization and momentum of the second soft photon, and $\mathcal{M}_\gamma$ is the LO amplitude for the single photon emission. The differential decay rate, $d\Gamma_{\gamma\gamma}$, for the double photon emission, integrated over the soft photon phase space, is

$$d\Gamma_{\gamma\gamma} = -\frac{\alpha}{\pi}\left\{\left(\ln y_{\min}^2 - \ln\frac{\lambda^2}{m_\tau^2}\right)\left[1+\frac{x}{\sqrt{x^2-4r^2}}\ln\left(\mathcal{X}_1\right)\right] + \frac{x}{\sqrt{x^2-4r^2}}\left[\ln^2\left(\mathcal{X}_1\right)+\ln\left(\mathcal{X}_1\right)+\mathrm{Li}_2\left(\frac{2\sqrt{x^2-4r^2}}{x+\sqrt{x^2-4r^2}}\right)\right]-1\right\} d\Gamma_\gamma. \tag{1.71}$$

where $y_{\min} = 2E_{\min}/m_\tau$ is the normalized photon energy threshold, λ is the fictitious photon mass, $d\Gamma_\gamma$ is the LO differential decay rate in Eq. (1.63) and

$$\mathcal{X}_1 = -\frac{x-2r-\sqrt{x^2-4r^2}}{x-2r+\sqrt{x^2-4r^2}}. \tag{1.72}$$

Our result in (1.71) agrees with those in Refs. [81, 112]. In the end, we verified that IR poles arising from virtual correction cancel out with those appearing in real photon emission.

1.9.3 NLO prediction and comments

The differential decay rate for $\tau \to l\nu_\tau\bar{\nu}_l\gamma$ at NLO in QED is

$$\frac{d^6\Gamma^{\mathrm{NLO}}}{dx\,dy\,d\Omega_l\,d\Omega_\gamma} = \frac{\alpha\,G_F^2 m_\tau^5}{(4\pi)^6}\frac{x\beta}{1+\delta_{\mathrm{W}}(m_\mu,m_e)} \times\left[G(x,y,c)+x\beta\,\hat{n}\cdot\hat{p}_l\,J(x,y,c)+y\,\hat{n}\cdot\hat{p}_\gamma\,K(x,y,c)+y\,x\beta\,\hat{n}\cdot(\hat{p}_l\times\hat{p}_\gamma)\,L(x,y,c)\right]. \tag{1.73}$$

The function $G(x, y, c)$, and similarly for J and K, is given by

$$G(x, y, c) = \frac{4}{3yz^2}\left[g_{\rm LO}(x, y, z) + \frac{\alpha}{\pi}\, g_{\rm NLO}(x, y, z; y_{\rm min}) + r_{\rm W}^2\, g_{\rm W}(x, y, z)\right], \tag{1.74}$$

where $g_{\rm LO}(x, y, z)$ and $g_{\rm W}(x, y, z)$ are the tree-level contributions, as described before in Sec. 1.8, and $g_{\rm NLO}(x, y, z; y_{\rm min})$ contains both virtual and real QED corrections. We explicitly verified the results to be free from both UV and IR divergences. For clarity here, we omitted those terms involving the dipole moments. The function $L(x, y, z)$, appearing in front of the $\hat{n}\cdot(\hat{p}_l \times \hat{p}_\gamma)$ term, is purely induced by loop corrections and thus is of $\mathcal{O}(\alpha/\pi)$. As a matter of fact, $L(x, y, z)$ is of the form $\sum_n P_n(x, y, z)\mathrm{Im}\left[I_n(x, y, z)\right]$, where the P_n are polynomials in x, y, z and $I_n(x, y, z)$ are scalar integrals whose imaginary part is different from zero.

QED one-loop corrections to muon (tau) leptonic radiative decay were computed before in [111, 112, 119] with various levels of completeness and precision. In the unpublished study of Ref. [119] the integrals are either taken from external sources or left in an implicit form for numerical evaluation. This situation rendered in practice the final comparison impossible to carry out. In [111] only the isotropic corrections $g_{\rm NLO}$, independent on $\hat{n}$, were computed and we also found several typos. Moreover we did manage to get hold of their expression.

Authors in [112] performed the calculation with full spin dependence, but in the $r = m_l/m_\tau \to 0$ limit. They provided us with their prediction for the differential decay rate in a Fortran code. We compared the numerical values of $g_{\rm NLO}$, $j_{\rm NLO}$, $k_{\rm NLO}$ and $L_{\rm NLO}$ in tens of (x, y, c)-phase space points. Our result perfectly agrees in the isotropic part $g_{\rm NLO}$ (better than per mil level), while we found two important discrepancies in the sector dependent on the tau spin direction $\vec{n}$. We have numerical disagreement for the functions $j_{\rm NLO}$ and $k_{\rm NLO}$. Also, in the NLO decay rate formula of [112], equivalent to our expression (1.73), that function $L(x, y, z)$, in front of the $\hat{n}\cdot(\hat{p}_l \times \hat{p}_\gamma)$ term, does not appear. From our previous discussion, $L(x, y, z)$ may vanish if one erroneously assumes the scalar integrals to be real quantities, which is not true in general. We also checked that the $L(x, y, z)$ does not vanish numerically, neither it goes to zero in the $r \to 0$ limit.

Throughout our calculation we performed two types of consistency checks. To test the calculation of the one-loop amplitude, $\varepsilon^*_\mu(p_\gamma)\mathcal{M}^\mu_{\rm virt}$, we explicitly verified that after renormalization $\mathcal{M}^\mu_{\rm virt}$ satisfies the Ward identity,

$$p_{\gamma\,\mu}\mathcal{M}^\mu_{\rm virt} = 0, \tag{1.75}$$

where $\epsilon^*_\mu(p_\gamma)$ is the polarization vector of the out-going photon whose momentum is p_γ.

This is also true separately for the two subsets of gauge-invariant diagrams in Figs. 1.10a-c and Figs.1.10b-d. The second test involved the weak current, spin projectors and the treatment of γ_5 in dimensional regularization. We used the standard scheme $\{\gamma^\mu, \gamma_5\} = 0$. Another way to treat consistently the γ_5 is to renounce dimensional regularization. Since we had to deal only with one-loop integrals, it appeared worthwhile to derive with small effort the NLO sector of (1.73) in the $D = 4$ Pauli-Villars regularization scheme. We found perfect agreement with the expressions evaluated in dimensional regularization.

1.10 Branching Ratios

In this section we report results for the branching ratios of tau leptonic decays. We implemented the analytic expression for Eq. (1.73) in C and Fortran codes, used in the feasibility study of Sec. 1.11 and for evaluation of partial widths.

The kinematic limits for x, c, and y are

$$2r \le x \le 1 + r^2, \quad -1 \le c \le 1, \tag{1.76}$$

$$0 < y \le y_{\max}(x, c), \tag{1.77}$$

where the maximum normalized photon energy is

$$y_{\max}(x, c) = \frac{2\left(1 + r^2 - x\right)}{2 - x + c\,x\beta}. \tag{1.78}$$

However, every experimental setup has a minimum photon energy $E_\gamma^{\min} = y_{\min}(m_\tau/2)$ below which photons are not detected. As the constraint $y_{\min} < y_{\max}(x, c)$, necessary to measure radiative decays, leads to the bound $c < c_{\max}(x)$, with

$$c_{\max}(x) = \frac{2\left(1 + r^2 - x\right) - \left(2 - x\right) y_{\min}}{x\beta\, y_{\min}}, \tag{1.79}$$

the kinematic ranges of x, c, and $y > y_{\min}$ are reduced to

$$2r \le x \le 1 + r^2, \quad -1 \le c \le \min\{1, c_{\max}(x)\}, \tag{1.80}$$

$$y_{\min} \le y \le y_{\max}(x, c). \tag{1.81}$$

We noted that the terms in G, J, and K proportional to r^2 cannot be neglected in the integrated decay rate. Indeed, the functions multiplying these r^2 terms generate a singular behavior in the $r \to 0$ limit after the integration over $c \equiv \cos\theta$: terms proportional to r^2/z^2 in G (or J, K) lead to a nonvanishing contribution to the integrated

process	B.R. (LO)	exp. B.R.
$\mu^+ \to e^+\nu_e\bar{\nu}_\mu\gamma$	1.3×10^{-2}	$1.4\,(4) \times 10^{-2}$
$\tau^- \to e^-\bar{\nu}_e\nu_\tau\gamma$	1.84×10^{-2}	$(1.75 \pm 0.06 \pm 0.17) \times 10^{-2}$
$\tau^- \to \mu^-\bar{\nu}_\mu\nu_\tau\gamma$	3.67×10^{-3}	$(3.61 \pm 0.16 \pm 0.35) \times 10^{-3}$

TABLE 1.4: Branching ratios of radiative muon and tau decays for a photon energy threshold $E_\gamma^{\rm min} = 10$ MeV. Experimental value for the decay of μ^+ is from Ref. [123]. A new preliminary measurement of this branching ratio has recently been reported by the MEG experiment [124]. The values for τ^- were measured by the CLEO Collaboration, where the first error is statistical and the second one is systematic [125].

process	B.R. (LO)	B.R. (NLO)	B.R. (NLO)/B.R. (LO)
$\mu^+ \to e^+\nu_e\bar{\nu}_\mu\gamma$	1.31×10^{-2}	-1.1×10^{-4}	-0.8%
$\tau^- \to e^-\bar{\nu}_e\nu_\tau\gamma$	1.836×10^{-2}	-1.83×10^{-3}	-10%
$\tau^- \to \mu^-\bar{\nu}_\mu\nu_\tau\gamma$	3.67×10^{-3}	-9.1×10^{-5}	-2.5%

TABLE 1.5: Contributions to the branching ratios given by the NLO corrections $(\alpha/\pi)g_{\rm NLO}$ in (1.74), and ratios to the LO. The photon energy threshold is $E_\gamma^{\rm min} = 10$ MeV.

decay rate since $\int dc\,(1/z^2) \propto 1/z$ is evaluated at the integration limit $c \to 1$ where $z \to xy\,(1-\beta)/2 \approx r^2(y/x)$ for $x \gg 2r$. If the initial $\mu^\pm$ or $\tau^\pm$ are not polarized, Eq. (1.73) simplifies to

$$\frac{d^3\Gamma}{dx\,dc\,dy} = \frac{\alpha G_F^2 m_\tau^5}{(4\pi)^6}\,\frac{8\pi^2\,x\beta}{1+\delta_{\rm W}(m_\mu,m_e)}\,G(x,y,c). \tag{1.82}$$

Integrating Eq. (1.82) over the kinematic ranges (1.80) and dividing the result by the muon or tau total widths $\Gamma_{\mu,\tau}$ one obtains the branching ratios of the radiative decays (1.62) for a given threshold $y_{\rm min}$. We noted that these branching ratios contain mass singularities (and $\ln y_{\rm min}$) [90, 120], but their presence does not contradict the Kinoshita–Lee–Nauenberg theorem, which applies only to total decay rates [81, 121, 122].

The branching ratio for radiative muon and tau decays, with a minimum detected photon energy $E_\gamma^{\rm min} = 10$ MeV, are reported in Tab. 1.4 and compared with current experimental values [123, 125]. Montecarlo integration has been performed with the `Cuba` library [126]. The relative contributions to the branching ratios arising from the isotropic terms $g_{\rm LO}, g_{\rm W}$ and $g_{\rm NLO}$ are shown in Tabs. 1.5 and 1.6. In tau radiative decays, NLO corrections give a -10% correction, for $l = e$, and -2.5% correction, for $l = \mu$. These corrections receive enhancement from soft and collinear emission through the logarithms $\ln y_{\rm min}$ and $\ln r$. The effects of the W-boson propagator are small and of $\mathcal{O}(10^{-4})$. However, we want to emphasize that the lack of these contributions in the decay rate, even if small, would turn out to be an extra source of systematic uncertainty in the experimental analysis.

process	B.R. (LO)	B.R. ($M_{\rm W}$)	B.R. ($M_{\rm W}$)/ B.R. (LO)
$\mu^+ \to e^+\nu_e\bar{\nu}_\mu\gamma$	1.31×10^{-2}	1.5×10^{-8}	$\mathcal{O}(10^{-6})$
$\tau^- \to e^-\bar{\nu}_e\nu_\tau\gamma$	1.836×10^{-2}	5.7×10^{-6}	3×10^{-4}
$\tau^- \to \mu^-\bar{\nu}_\mu\nu_\tau\gamma$	3.67×10^{-3}	1.2×10^{-6}	3×10^{-4}

TABLE 1.6: Contributions to the branching ratios given by the W-boson effect $r_{\rm W}^2 g_{\rm W}$ in (1.74), and ratios to the LO. The photon energy threshold is $E_\gamma^{\rm min} = 10$ MeV.

Contributions to the partial widths arising from the effective operators (1.45) are very tiny compared to the LO. For example the additional contributions from $g-2$ coupling to the branching ratios are $[(8.6\times10^{-4})\tilde{a}_\tau]\%$ (for $l = e$) and $[(8.2\times10^{-4})\tilde{a}_\tau]\%$ (for $l = \mu$). Branching ratios are too inclusive quantities to be sensitive on tau dipole moments: their contributions are killed by integration, mainly because the G term in (1.73) behaves like $1/E_\gamma^2$ at small photon energy, while G_a does not. Only exploiting the full phase space one can have a chance to disentangle these tiny effects. Indeed, the method of unbinned maximum likelihood, described in the next section, basically fits the triple differential decay rate in Eq. (1.73), i.e. it aims precisely to use the maximum amount of available information from every single radiative decay event.

1.11 Feasibility study at Belle and Belle-II[†]

In this section we outline the technique applied for estimating the future sensitivity on tau dipole moments in leptonic radiative decays.

As it was suggested in [72] we performed a feasibility study of the $\tilde{a}_\tau$ in the vicinity of the radiation zero point in the phase space of $\tau \to \ell\nu\nu\gamma$ ($\ell = e,\ \mu$) decay ($\cos\widehat{(\ell,\gamma)} = -1$, $x = 2E_\ell^{\rm max}/m_\tau = 1 + m_\ell^2/m_\tau^2$). For that we analyzed a set of $\tau^+\tau^-$ events, where one τ decays to the radiative leptonic mode and the other τ decays to ordinary leptonic mode, ($\tau^\pm \to \ell_1^\pm\nu\nu\gamma,\ \tau^\mp \to \ell_2^\mp\nu\nu$), $\ell_{1,2} = e,\mu$; $\ell_1 \neq \ell_2$, or shortly ($\ell_1^\pm\gamma,\ \ell_2^\mp$). We excluded ($e^\pm\gamma,\ e^\mp$) and ($\mu^\pm\gamma,\ \mu^\mp$) events from our analysis due to the large background from $e^+e^- \to e^+e^-\gamma$ and $e^+e^- \to \mu^+\mu^-\gamma$ processes. Analyzed events were produced by KKMC/TAUOLA/PHOTOS generators [128–130] and processed by GEANT3 based program [131] in the conditions of the Belle experiment [132–135].

The sensitivity to $\tilde{a}_\tau$ is determined by the background suppression power $\varepsilon_{\rm sig}/\varepsilon_{\rm bg}$, where $\varepsilon_{\rm sig}$ is the detection efficiency for signal events and $\varepsilon_{\rm bg}$ is detection efficiency for background events. The main background comes from the ordinary radiative leptonic decays (characterized by $\tilde{a}_\tau = 0$) as well as from ($\tau^+ \to \ell_1^+\nu\nu;\ \tau^- \to \ell_2^-\nu\nu)\gamma_{\rm ISR}$ events with initial state radiation (ISR) to the large polar angles in the detector. As the fraction of

[†]work in collaboration with D. Epifanov, C. Ng, F. Okazawa [127]

the signal events in the vicinity of the radiation zero point is very small, we extended the signal region to maximize $\varepsilon_{\rm sig}/\varepsilon_{\rm bg}$:

$$0.1 < \cos\widehat{(\ell_2,\gamma)} < 0.8, \quad \cos\widehat{(\ell_1,\gamma)} < -0.9, \quad \text{and } E_\gamma > 0.5 \text{ GeV}. \tag{1.83}$$

Even in this case, the $\tilde{a}_\tau$ upper limit, which can be achieved with the whole Belle statistics of about 0.9×10^9 τ pairs, is only UL$(\tilde{a}_\tau) \simeq 2$. We found that the phenomenon of radiation zero has no large influence on the $\varepsilon_{\rm sig}/\varepsilon_{\rm bg}$. The dynamical structure of the signal events, determined by $G_a(x,y,c)$ and $G_{aa}(x,y,c)$ form factors, allows us to achieve $\varepsilon_{\rm sig}/\varepsilon_{\rm bg} \sim 100$ only. At the same time the suppression of the signal branching fraction (for $\tilde{a}_\tau = 1$) is $\mathcal{B}_{\rm bg}/\mathcal{B}_{\rm sig} \simeq 2000$, i.e. about one order of magnitude larger than $\varepsilon_{\rm sig}/\varepsilon_{\rm bg}$. As a result there is no possibility to improve essentially the $\tilde{a}_\tau \sim 1$ sensitivity.

The other more complicated and most powerful method to extract $\tilde{a}_\tau$ and $\tilde{d}_\tau$ is an unbinned maximum likelihood fit of events in the full phase space. The main idea of this method is to consider events where both taus decay to particular final states. One $\tau^\mp$ (signal side) decays to radiative leptonic mode and the other $\tau^\pm$ (tag side) decays to some well investigated mode with large branching fraction. As a tag decay mode we choose $\tau^\pm \to \rho^\pm\nu \to \pi^\pm\pi^0\nu$, which also serves as spin analyser and allows us to be sensitive to the spin dependent part of the differential decay width of signal decay using effects of spin-spin correlation of taus [136]. With this technique we analyzed $(\ell^\mp\nu\nu\gamma,\ \pi^\pm\pi^0\nu)$ events in the 12-dimensional phase space (PS).

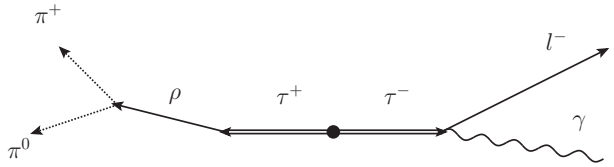

FIGURE 1.11: the ρ-tag mode applied in the unbinned maximum likelihood fit. Events are analyzed in the 12-dimensional phase space of $(\ell^\mp, \gamma, \pi^\pm, \pi^0)$. Undetected neutrinos are not drawn.

The probability density function (PDF) is constructed from the total differential cross section $\frac{d\sigma}{\rm dPS}(e^+e^- \to \tau^\mp\tau^\pm \to (\ell^\mp\nu\nu\gamma,\ \pi^\pm\pi^0\nu))$, which is a sum of spin independent term and spin-spin correlation term. To write the total differential cross section we followed the approach developed in [137, 138]. The differential cross section of $e^+e^- \to \tau^+(\vec{\zeta}^{*+})\tau^-(\vec{\zeta}^{*-})$ reaction in the center-of-mass system (c.m.s.) is given by formula [136]

$$\frac{d\sigma(\vec{\zeta}^{*-},\vec{\zeta}^{*+})}{d\Omega} = \frac{\alpha^2}{64E_\tau^2}\beta_\tau(D_0 + D_{ij}\zeta_i^{*-}\zeta_j^{*+}), \tag{1.84}$$

where $D_0 = 1 + \cos^2\theta + \sin^2\theta/\gamma_\tau^2$ and

$$D_{ij} = \begin{pmatrix} (1+\frac{1}{\gamma_\tau^2})\sin^2\theta & 0 & \frac{1}{\gamma_\tau}\sin 2\theta \\ 0 & -\beta_\tau^2\sin^2\theta & 0 \\ \frac{1}{\gamma_\tau}\sin 2\theta & 0 & 1+\cos^2\theta - \frac{1}{\gamma_\tau^2}\sin^2\theta \end{pmatrix}, \tag{1.85}$$

with $\vec{\zeta}^{*\mp}$ the polarisation vector of $\tau^\mp$ in the $\tau^\mp$ rest frame (unitary vector along $\tau^\mp$ spin direction). Asterisks indicate parameters measured in the associated τ rest frame. Moreover, α, E_τ, $\gamma_\tau = E_\tau/M_\tau$, $\beta_\tau = P_\tau/E_\tau$ and θ are the fine structure constant, the energy, the Lorentz factor, the velocity of τ (in the units of c) and the polar angle of the τ^- momentum direction respectively. The signal differential decay width is written in the form (with unimportant, for this analysis, total normalization constant $\kappa_{\ell\gamma}$):

$$\frac{d\Gamma(\tau^\mp(\vec{\zeta}^*) \to \ell^\mp\nu\nu\gamma)}{dx^* dy^* d\Omega_\ell^* d\Omega_\gamma^*} = \kappa_{\ell\gamma}\left[A(x^*,y^*,z^*) \mp \vec{\zeta}^* \cdot \vec{B}(x^*,y^*,z^*))\right], \tag{1.86}$$

where $A(x,y,z) = G(x,y,z)$ and

$$\vec{B} = \vec{n}_\ell^* x^* \beta^* J + \vec{n}_\gamma^* y^* K + [\vec{n}_\ell^* \times \vec{n}_\gamma^*] y^* x^* \beta^* L \tag{1.87}$$

The definitions of all variables in the last equations can be found in Sec. 1.8.

The $\tau^\pm(\vec{\zeta'}^*) \to \rho^\pm(K^*)\nu(q^*) \to \pi^\pm(p_1^*)\pi^0(p_2^*)\nu(q^*)$ decay width reads (with the total normalization constant κ_ρ):

$$\frac{d\Gamma(\tau^\pm \to \pi^\pm\pi^0\nu)}{dm_{\pi\pi}^2 d\Omega_\rho^* d\tilde{\Omega}_\pi} = \kappa_\rho(A' \mp \vec{B}'\vec{\zeta'}^*)W(m_{\pi\pi}^2), \tag{1.88}$$

where

$$\begin{aligned} A' &= 2\,q\cdot Q\,Q_0^* - Q^2 q_0^*, & \vec{B}' &= Q^2\vec{K}^* + 2\,q\cdot Q\,\vec{Q}^*, \\ Q^* &= p_1^* - p_2^*, & K^* &= p_1^* + p_2^*, \\ W(m_{\pi\pi}^2) &= |F_\pi(m_{\pi\pi}^2)|^2 \frac{p_\rho(m_{\pi\pi}^2)\tilde{p}_\pi(m_{\pi\pi}^2)}{M_\tau m_{\pi\pi}}, & m_{\pi\pi}^2 &= K^{*2}, \\ p_\rho &= \frac{M_\tau}{2}\left(1 - \frac{m_{\pi\pi}^2}{M_\tau^2}\right), & \tilde{p}_\pi &= \frac{\lambda^{\frac{1}{2}}(m_{\pi\pi}^2, m_\pi^2, m_{\pi^0}^2)}{2m_{\pi\pi}}. \end{aligned} \tag{1.89}$$

Here we used the Källen function $\lambda(x,y,z) \equiv x^2+y^2+z^2-2xy-2xz-2yz$. Also p_ρ and Ω_ρ^* are momentum and solid angle of ρ meson in the τ rest frame, $\tilde{p}_\pi$ and $\tilde{\Omega}_\pi$ the momentum and solid angle of charged pion in the ρ rest frame, and $F_\pi(m_{\pi\pi}^2)$ is the pion form factor with CLEO parameterisation [139]. As a result, the total differential cross

section for $(\ell^{\mp}\gamma, \rho^{\pm})$ events can be written as [136]

$$\frac{d\sigma(\ell^{\mp}\gamma, \rho^{\pm})}{dE^*_\ell d\Omega^*_\ell dE^*_\gamma d\Omega^*_\gamma d\Omega^*_\rho dm^2_{\pi\pi} d\tilde{\Omega}_\pi d\Omega_\tau} = \kappa_{\ell\gamma}\kappa_\rho \frac{\alpha^2\beta_\tau}{64E^2_\tau}\left(D_0 A' A + D_{ij}B_i B'_j\right)W. \tag{1.90}$$

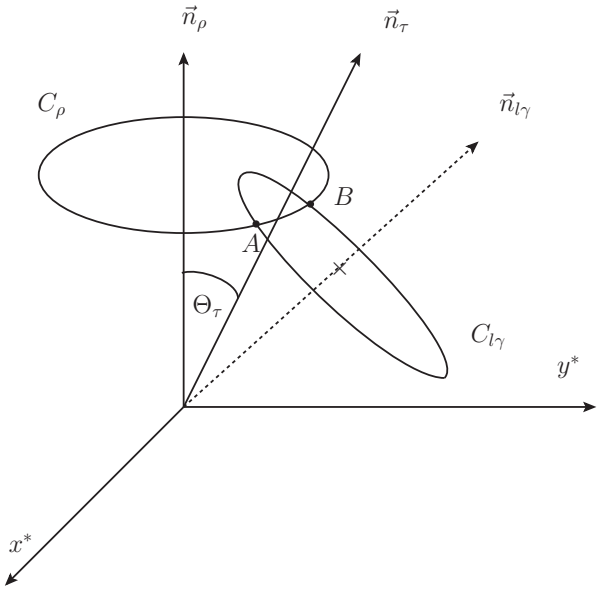

FIGURE 1.12: Configuration of the two circles C_ρ and $C_{l\gamma}$ on a unit sphere, which are determined from the decay $\tau^+ \to \rho^+\nu$ and $\tau^- \to l^-\nu\bar{\nu}\gamma$, respectively. The kinematically allowed region for C_ρ is the circumference and the region $C_{l\gamma}$ is either inside or outside of the circle, depending on $\cos\Theta_\tau > 0$ or < 0

In the c.m.s. the $\tau^{\mp}$ directions are limited on a arc (Φ_A, Φ_B). The neutrino mass constraint in the decay $\tau^+ \to \rho^+\nu$ is written as $(p_\tau - p_\rho)^2 = 0$, which gives the τ^+ production angle, Θ_τ, with respect the ρ direction $\vec{n}_\rho$. This relation indicates that the τ^+ direction $\vec{n}_\tau$, which lies on a unit sphere, is on the circumference of a circle C_ρ with radius equal to $\sin\Theta_\tau$, as shown in Fig. 1.12. Similarly, the invariant mass $M_{\nu\bar{\nu}} > 0$ of the two neutrino system in the decay $\tau^- \to l^-\nu\bar{\nu}\gamma$ gives a constraint to Θ'_τ, where Θ'_τ is the τ angle along the direction of the $l\gamma$ system. The inequality $M_{\nu\bar{\nu}} > 0$ confines the vector $\vec{n}_\tau$ inside the circle $C_{l\gamma}$. Therefore, in the c.m.s., the direction of the $\tau^{\mp}$ system is given by the intersection between the circumference of C_ρ and the circle $C_{l\gamma}$, i.e. the arc (Φ_A, Φ_B).

Experimentally one measures particle parameters in the c.m.s., hence the visible differential cross section is given by [138]:

$$\mathcal{F}(p_\ell, \Omega_\ell, p_\gamma, \Omega_\gamma, p_\rho, \Omega_\rho, m^2_{\pi\pi}, \tilde{\Omega}_\pi) = \frac{d\sigma(\ell^{\mp}\gamma, \rho^{\pm})}{dp_\ell d\Omega_\ell dp_\gamma d\Omega_\gamma dp_\rho d\Omega_\rho dm^2_{\pi\pi} d\tilde{\Omega}_\pi} =$$

$$= \int_{\Phi_A}^{\Phi_B} \frac{d\sigma(\ell^{\mp}\gamma, \rho^{\pm})}{dE^*_\ell d\Omega^*_\ell dE^*_\gamma d\Omega^*_\gamma d\Omega^*_\rho dm^2_{\pi\pi} d\tilde{\Omega}_\pi d\Omega_\tau} \left|\frac{\partial(E^*_\ell, \Omega^*_\ell, E^*_\gamma, \Omega^*_\gamma, \Omega^*_\rho, \Omega_\tau)}{\partial(p_\ell, \Omega_\ell, p_\gamma, \Omega_\gamma, p_\rho, \Omega_\rho, \Phi_\tau)}\right| d\Phi_\tau, \tag{1.91}$$

where the integration is done over the unknown tau direction, which is constrained on the (Φ_A, Φ_B) arc. Both Φ_A and Φ_B angles are calculated using parameters measured in the experiment. The Jacobian in Eq.(1.91) can be further simplified as:

$$\left|\frac{\partial(E^*_\ell, \Omega^*_\ell, E^*_\gamma, \Omega^*_\gamma, \Omega^*_\rho, \Omega_\tau)}{\partial(p_\ell, \Omega_\ell, p_\gamma, \Omega_\gamma, p_\rho, \Omega_\rho, \Phi_\tau)}\right| = \left|\frac{\partial(E^*_\ell, \Omega^*_\ell)}{\partial(p_\ell, \Omega_\ell)}\right| \cdot \left|\frac{\partial(E^*_\gamma, \Omega^*_\gamma)}{\partial(p_\gamma, \Omega_\gamma)}\right| \cdot \left|\frac{\partial(\Omega^*_\rho, \Omega_\tau)}{\partial(p_\rho, \Omega_\rho, \Phi_\tau)}\right|, \qquad (1.92)$$

where the expressions for the latter Jacobians can be found in [138].

TABLE 1.7: Sensitivities to $\tilde{a}_\tau$ and $\tilde{d}_\tau$ in radiative leptonic decays of τ (ρ-tag and full tag cases), which can be achieved with the whole data sample collected at Belle and planned in Belle II experiment. Values for $\tilde{d}_\tau$ are in natural units of m_τ. Results of the previous most precise studies done at DELPHI and Belle are also shown in the last two lines.

	$\mathrm{Re}(\tilde{a}_\tau)$	$\mathrm{Im}(\tilde{a}_\tau)$	$\mathrm{Re}(\tilde{d}_\tau)$	$\mathrm{Im}(\tilde{d}_\tau)$
Belle (ρ-tag)	0.16	0.16	0.15	0.046
Belle-II (ρ-tag)	0.023	0.023	0.021	0.007
Belle (full tag)	0.085	0.085	0.080	0.024
Belle-II (full tag)	0.012	0.012	0.011	0.003
DELPHI	0.017	—	—	—
Belle	—	—	0.0015	0.0008

In our feasibility study we developed a special generator of the signal ($\ell^\mp\nu\nu\gamma$, $\pi^\pm\pi^0\nu$) events. For the unbinned maximum likelihood fit of the generated events the PDF is constructed as ($\vec{X} = (p_\ell, \Omega_\ell, p_\gamma, \Omega_\gamma, p_\rho, \Omega_\rho, m^2_{\pi\pi}, \tilde{\Omega}_\pi)$):

$$\mathcal{P}(\vec{X}) = \frac{\mathcal{F}(\vec{X})}{\int \mathcal{F}(\vec{X}) d\vec{X}}. \qquad (1.93)$$

By fitting samples of generated events corresponding to the amount of data available at Belle [132–135] and expected at Belle II [67, 140] we studied the sensitivities to parameters $\tilde{a}_\tau$ and $\tilde{d}_\tau$.

The obtained results are collected in Tab. 1.7 where the sensitivities are shown for two cases: (i) events are tagged by $\tau^\pm \to \rho^\pm\nu$ only (ρ-tag), (ii) six decay modes ($\tau^\pm \to \rho^\pm\nu$, $\tau^\pm \to \pi^\pm\nu$, $\tau^\pm \to \pi^\pm\pi^0\pi^0\nu$, $\tau^\pm \to \pi^\pm\pi^+\pi^-\nu$, $\tau^\pm \to e^\pm\nu\nu$, $\tau^\pm \to \mu^\pm\nu\nu$) with a total branching fraction of about 90% are used for the tag (full tag). In the full-tag case, the sensitivity increase is due to the statistical factor $\sqrt{90/25.5} = 1.88$, compared to the ρ-tag case with B.R.= 25.5%). We noted that the integration over (Φ_A, Φ_B) arc inflates the uncertainty by a factor of 1.4, in comparison with the case when the direction of the tau is known. Also, the inclusion of the spin dependent part of the differential decay width increases the sensitivity by a factor ~ 1.5. It is interesting to note that for events with $\tau \to e\nu\bar{\nu}\gamma$ the sensitivity is two times worse than for $\tau \to \mu\nu\bar{\nu}\gamma$ (for the same

statistics). In Tab. 1.7 the sensitivities to $\tilde{a}_\tau$ and $\tilde{d}_\tau$ obtained in the previous most precise studies at DELPHI [17] and Belle [19] are also shown for the comparison. It is clearly seen that the measurement of $\mathrm{Re}(\tilde{a}_\tau)$ and $\mathrm{Im}(\tilde{a}_\tau)$ in τ radiative leptonic decays at Belle II with the full tag can be already competitive with the DELPHI result, on the other hand the expected sensitivity to $\mathrm{Re}(\tilde{d}_\tau)$ and $\mathrm{Im}(\tilde{d}_\tau)$ is still worse than the most precise measurement of $\tilde{d}_\tau$ done at Belle in $\tau^+\tau^-$ pair production.

Chapter 2

Probing top quark dipole moments in single-top+γ production

2.1 Introduction

In view of its large mass the top quark is a unique probe of the dynamics that break the electroweak gauge symmetry. While the observation of a Higgs boson at the CERN LHC [141, 142] and first measurements of its production and decay channels appear to be consistent with the Standard Model (SM) Higgs mechanism of electroweak symmetry breaking, this mechanism is still far from being validated at high precision. Deviations from the SM are likely to be most pronounced in processes involving top quarks. They may become manifest as deviations of the top-quark gauge-boson couplings from the values predicted by the SM (see [5, 6] for overviews).

Several studies have established photon radiation in top quark pair production at hadron colliders as potential probe of anomalous coupling effects [9], which could be improved upon only at a future high-energy electron-positron collider by exploiting final state correlations [10] in top quark pair production. The production of $t\bar{t}\gamma$ final states was first measured at the Tevatron [143], and studies at the LHC are ongoing [144, 145]. While indirect constraints on anomalous electromagnetic couplings from electroweak precision data or flavour physics observables turn out to be very constraining for bottom quarks [11–13], only loose bounds can be obtained in the case of top quarks (see [14, 15] for recent studies).

At the LHC the cross sections for top quark pair production and single top quark production are of comparable magnitude. It is the aim of this chapter to extend the considerations made in [9] for $t\bar{t}\gamma$ production to photon radiation in single-top production and to estimate the sensitivity of single-top-plus-photon events to the anomalous electromagnetic couplings of the top quark. In Sec. 2.2, we review the current theoretical determination the photon-top vertex, and then we introduce its effective field theory parametrization (Sec. 2.3). The parton-level phenomenology of these new operators is then discussed in Sec. 2.4, followed by numerical results for signal and background processes contributing to single-top-plus-photon production at the LHC in view of a determination of anomalous couplings in this process (Sec. 2.5). These results are used in Section 2.6 to quantify the sensitivity of future LHC data.

2.2 SM prediction of the top dipole moments

Let us review the SM prediction for the top dipole moments and the current experimental determinations. The top form factors, appearing in (1.1), can be computed order-by-order in perturbation theory: for heavy quarks they are known to one loop in the electroweak theory [42, 146, 147] and two loops in QCD [148–150]. The quantities $F_{2V}(0)$ and $F_{2A}(0)$ are related to the top $g-2$ and EDM through the identities in Eq. 1.2. The SM values for the static dipole moments can be derived from the form factors results. It is important to note that, compared to the case of leptons, the anomalous magnetic moment of a quark, a_Q, receives the largest contribution from QCD corrections. The QCD contributions to the heavy quark $g-2$ are known up to three-loop level:

$$a_Q^{\mathrm{QCD}} = \frac{\alpha_s}{2\pi} C_F + \left(\frac{\alpha_s}{2\pi}\right)^2 A_Q^{(2l)} + \left(\frac{\alpha_s}{2\pi}\right)^3 A_Q^{(3l)} + \mathcal{O}\left(\alpha_s^4\right), \tag{2.1}$$

where the QCD coupling $\alpha_s = \alpha_s(\mu)$, with μ the renormalization scale, is defined in the standard $\overline{\mathrm{MS}}$ scheme with N_l massless quarks and one quark Q with mass m_Q. The

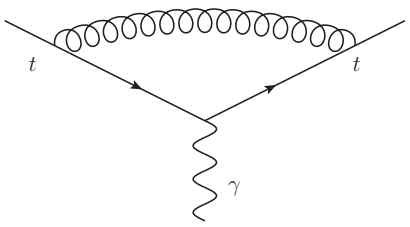

FIGURE 2.1: the leading contribution to the top $g-2$.

leading contribution arises from the one-loop digram in Fig. 2.1, where a virtual gluon is exchanged (instead of a virtual photon as in the case of a lepton). The mass independent

result is [151]

$$a_q^{\mathrm{LO}} = \frac{\alpha_s}{2\pi} C_F, \tag{2.2}$$

in analogy with the leading contribution to the electron $g-2$: $\alpha_{\mathrm{em}}/(2\pi)$ [29].

The two-loop QCD contribution has the analytic compact form [151]:

$$\begin{aligned} A_Q^{(2l)} = {} & C_F^2 \left(-\frac{31}{4} + 2\,\zeta_2\,(5 - 6\ln(2)) + 3\,\zeta_3 \right) \\ & + C_F\,C_A \left(\frac{317}{36} + 3\,\zeta_2\,(-1 + 2\ln(2)) - \frac{3}{2}\zeta_3 \right) \\ & + C_F T_F \left(\frac{119}{9} - 8\,\zeta_2 \right) - \frac{25}{9} C_F T_F N_l + C_F \beta_0 \ln\left(r_Q\right), \end{aligned} \tag{2.3}$$

where $r_Q = \mu^2/m_Q^2$, ζ_n is the Riemann zeta function, and $C_F = (N_c^2-1)/2N_C$, $C_A = N_c$, $T_F = 1/2$ with $N_c = 3$ being the number of colors. Furthermore $\beta_0 = (11C_A - 4T_F(N_l + 1)/6)$. The analytic expression for the three-loop QCD coefficient $A_Q^{(3l)}$ was computed in [152], but it is not reported here.

	$t \quad (\mu = m_t)$	$b \quad (\mu = m_b)$
$a_Q^{(1l)}$ [151]	$2.29 \cdot 10^{-2}$	$4.55 \cdot 10^{-2}$
$a_Q^{(2l)}$ [151]	$7.1 \cdot 10^{-3}$	$3.01 \cdot 10^{-2}$
$a_Q^{(3l)}$ [152]	$2.5 \cdot 10^{-3}$	$2.43 \cdot 10^{-2}$
a_Q	$3.25 \cdot 10^{-2}$	$7.56 \cdot 10^{-2}$

TABLE 2.1: One-, two- and three-loop QCD contributions, and their sum, to the anomalous magnetic moments of the top and bottom quark.
Input values are $m_t = 175$ GeV, $m_b = 5$ GeV, $\alpha_s(m_t) = 0.1080$, $\alpha_s(m_b) = 0.2145$ [151].

Numerical results for the case of the bottom and top quark are shown in Tab. 2.1 where in the case $Q = t$, values are computed in $N_f = N_l + 1$ flavour QCD with $N_l = 5$, i.e. all quarks but the top taken to be massless, while for $Q = b$ it is assumed $m_i = 0$ $(i = u, d, s, c)$ and $m_b \neq 0$. Two-loop contribution to a_t and a_b are about 30 and 70 percent of the respective leading terms of order α_s. Also, three-loop correction sizes are not negligible fraction of the two-loop ones. For the top quark they represent a 10% of the total anomalous moment, whereas for the bottom they give a 30% correction.

The QED and electroweak corrections are subleading with respect to the QCD one. The first QED contribution, equivalent to that one in Eq. (1.11), is

$$a_Q^{\mathrm{QED}} = Q^2 \frac{\alpha_{\mathrm{e.m.}}}{2\pi}, \tag{2.4}$$

where Q is the heavy quark charge and $\alpha_{\mathrm{e.m.}}$ is the fine structure constant. In the case of top quark, QED contribution is of $\mathcal{O}(10^{-3})$, i.e. of the same order of magnitude of the three loop QCD corrections.

Top quark EDM is generated thorough CP-violating amplitudes that involve the element of the CKM matrix. In analogy with what we described in Sec. 1.4, fundamental top quark EDM arises starting from three-loop diagrams, of $\mathcal{O}(\alpha_s G_F^2)$ [153, 154]. The value for d_t can be estimated rescaling the EDM of the u-quark in [154]:

$$|d_t^{\rm SM}| < 10^{-31} - 10^{-32}\, e \cdot \text{cm}, \tag{2.5}$$

too small to be observable. EDM is potentially sensitive to new physics effects in the top quark sector, which could yield potentially large contributions. In extensions of the SM, e.g. MHDM and SUSY models, the d_t can arise at the one-loop level and, as a result, the typical top EDM is of the order of $10^{-18} - 10^{-20}\, e$·cm [5, 6, 155, 156] which is larger than the SM prediction by more than ten orders of magnitude. The enhancement due to the large top mass is particularly evident in some models with an extended Higgs sector for which the dipole moments often scale as m_f^3 [157].

2.2.1 Experimental bounds

The $tt\gamma$ coupling (and also the ttZ) cannot be constrained at hadron colliders via the measurement of the $t\bar{t}$ pair production with an intermediate virtual γ (or Z boson) since the cross section for $pp \to t\bar{t}$ is dominated by processes involving QCD coupling. The $tt\gamma$ coupling may then be measured via analysis of direct production to $t\bar{t}$ pairs in association with a photon. The best constraints on top anomalous couplings can at present be obtained from a combination of the direct production processes and flavour physics observables. Direct $t\bar{t}\gamma$ production was measured by CDF [143] and also recently reported by CMS and ATLAS [144, 145]. In addition CDF performed a measurements of the $t\bar{t}$ production cross section with the same selection criteria (but without a photon). In this way they determined the ratio $R = \sigma_{t\bar{t}\gamma}/\sigma_{t\bar{t}}$, in which the systematic uncertainties are eliminated.

In [15] the authors considered the branching ratios of $B \to X_s\gamma$ as well as $A_{CP}(B \to X_s\gamma)$ as a tool to extract the top moments. They also studied the ratio R as a function of the top $g-2$ and EDM to set bounds on those parameters by comparing it with the CDF result. However they concluded that indirect bounds arising from flavour physics are still more stringent than those obtained from the measurement of the ratio R at Tevatron. The estimated bounds read [15]:

$$\begin{aligned} -3.0 < \quad & a_t \quad < 0.45\ , \\ -0.29 \times 10^{-16}\, e\,\text{cm} < \quad & d_t \quad < 0.86 \times 10^{-16}\, e\,\text{cm}\ . \end{aligned} \tag{2.6}$$

2.3 Effective field theory approach to top quark dipole moments

Following the approach previously shown for the case of tau lepton, also discussed in [15, 158–160], we chose to describe the phenomenology of dipole moments in top production via an effective Lagrangian

$$\mathcal{L}_{\text{eff}} = \mathcal{L}_{\text{SM}} - \Delta a_t \frac{Q_t e}{4m_t} \bar{t}\sigma_{\mu\nu} t F^{\mu\nu} + i\frac{\Delta d_t}{2} \bar{t}\sigma_{\mu\nu}\gamma_5 t F^{\mu\nu}. \tag{2.7}$$

The couplings Δa_t and Δd_t are real and related to the top quark $g-2$ and EDM. They must be thought as arising after integrating out the heavy degrees of freedom associated to possible NP.

We recall that the Lagrangian (2.7) may be obtained in the framework of gauge-invariant effective operators. The large number and variety of dimension-six operators [73] lead to the appearance of many possible Lorentz structures for the top trilinear vertices, involving a large number of parameters:

$$\mathcal{L}_{\text{eff}} = \sum_i \frac{C_i}{\Lambda^2}\mathcal{O}_i. \tag{2.8}$$

Some of these operators are redundant and can be eliminated through the equation of motion [158]. As shown in [158, 161], in the case of electromagnetic dipole moments interactions, there are two, and only two, dimension-six gauge-invariant operators that give rise to both the $g-2$ and EDM,

$$\begin{aligned} \mathcal{O}^{33}_{uB\varphi} &= C^{33}_{uB\varphi}\bar{q}_{L3}\sigma^{\mu\nu} t_R \tilde{\varphi} B_{\mu\nu} + \text{h.c.}\,, \\ \mathcal{O}^{33}_{uW} &= C^{33}_{uW}\bar{q}_{L3}\sigma^{\mu\nu}\tau^a t_R \tilde{\varphi} W^2_{\mu\nu} + \text{h.c.}\,, \end{aligned} \tag{2.9}$$

where the coefficients $C^{33}_{uB\varphi}$ and C^{33}_{uW} are related to the parameters in (2.7) via

$$\Delta a_t \frac{Q_t}{4} = \frac{\sqrt{2}}{e}\text{Re}\left[c_W C^{33}_{uB\varphi} + s_W C^{33}_{uW}\right]\frac{v m_t}{\Lambda^2}, \tag{2.10}$$

$$\Delta d_t/2 = \frac{\sqrt{2}}{e}\text{Im}\left[c_W C^{33}_{uB\varphi} + s_W C^{33}_{uW}\right]\frac{v}{\Lambda^2}. \tag{2.11}$$

So phenomenological studies can be carried out using simpler Lagrangians, as the one in (2.7). It is interesting to note that the vector coupling γ^μ in Eq. (1.1) does not receive corrections from the dimension-six operators. Redundant operators, like $\mathcal{O}_{qW}, \mathcal{O}_{qB}$ and $\mathcal{O}_{uB}$ of Ref. [73], would yield corrections $\sim q^2 \bar{t}_L \gamma^\mu t_R$, but the redefinition of such operators eliminates such terms [158], so that corrections to the electromagnetic coupling are

absent. Additional q^2 terms in the form factors would arise from higher-dimensional operators (e.g. dimension-8 operators) and thus are further suppressed by power of q^2/Λ^2. For this reason it is important not to have the momentum in the process above the Λ scale, and thus in our case we will assume $\Lambda \gtrsim 1$ TeV.

2.4 Top quark dipole moments in single-top-plus-photon production*

The $tt\gamma$ coupling may be measured in the direct production of $t\bar{t}$ pairs or single-top with the emission of an extra photon. Bounds on the anomalous couplings can then be inferred by comparing sufficiently precise data to the cross sections modified by the interaction in Eq. (2.7). Their extraction in top quark pair production from $t\bar{t}\gamma$ final states was investigated in detail in Ref. [9]. These measurements can be complemented by single-top quark production processes. Indeed, with the cross sections for top pair production and single-top production being of comparable magnitude at the LHC (see Tab. 2.2), it appeared worthwhile to extend the $t\bar{t}\gamma$ production analysis in [9] to photon radiation in single top quark production.

process	$\sigma_{\rm tot}$ [pb] 7 TeV	$\sigma_{\rm tot}$ [pb] 14 TeV
$t\bar{t}$ [163]	172.0	953.6
single-top t-ch. [164]	41.7	151
single-antitop t-ch. [164]	22.5	92
$t\bar{t}\gamma$ [165, 166]	0.668	2.93
single-top+γ t-ch.	0.33	1.6
single-antitop+γ t-ch.	0.18	0.98

TABLE 2.2: Total cross section for $pp \to t\bar{t}(+\gamma)$ and single-top $(+\gamma)$ at the LHC operating at 7 and 14 TeV. The values reported here are for $m_t = 173$ GeV, factorization and renormalization scales are $\mu_F = \mu_R = m_t$. Isolated photons have $p_T(\gamma) > 20$ GeV. For clarity here the scale uncertainties are not reported. Single-top-plus-photon cross section has been estimated at NLO with `MadGraph5_aMC@NLO` [167]

Single top quark production at LHC is largely dominated by the t-channel process: $pp \to t + j$ with a light-quark jet in the final state [168, 169]. A potential probe of anomalous couplings in the top quark sector thus proceeds through the reaction

$$pp \to tj\gamma. \tag{2.12}$$

*work in collaboration with T. Gehrmann [162]

To quantify the potential effect of an anomalous magnetic moment of the top quark on this process, we first considered the parton-level reaction

$$ub \to td\gamma, \tag{2.13}$$

at fixed centre-of-mass energy, and in the rest frame of the incoming partons.

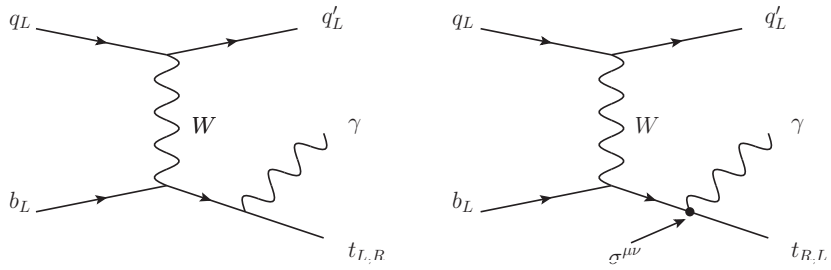

FIGURE 2.2: Photon radiation in $qb \to q't\gamma$ that involves the SM $tt\gamma$ coupling (left) and the effective dipole moment coupling (right). Diagrams with photons emitted by other charged particles are not depicted here. Top quarks coupled to the photon with the $\sigma^{\mu\nu}q_\nu$ coupling tend to have opposite chirality of those emitted through the SM γ^μ, unless a mass chirality-flip occurs.

Cross sections are obtained with a Fortran code generated by `FeynArts` and `FormCalc` [117, 170]. The new operators appearing in Eq. (1.44) are implemented in FeynArts with the Mathematica package `FeynRules` [171]. As we already mentioned in Sec. 1.2 direct production usually is not suited to disentangle $g-2$ effects from EDM, so for simplicity here we focus our discussion on the CP-conserving coupling $\Delta a_t \neq 0$ and set $\Delta d_t = 0$, knowing that all consideration can be actually extended also to the case $\Delta d_t \neq 0$. The total cross section σ for the reaction in Eq. (2.13) can be split in three contributions,

$$\sigma = \sigma_{\rm SM} + \Delta a_t \sigma_a + \Delta a_t^2 \sigma_{aa}, \tag{2.14}$$

where $\sigma_{\rm SM}$ is the leading-order Standard Model prediction, the term σ_a linear in Δa_t arises from the interference between Standard Model and the anomalous amplitudes, whereas the quadratic term σ_{aa} is the self-interference of the anomalous amplitudes.

We observe in Fig. 2.3 (left) that a contribution from the $g-2$ coupling gives a photon energy spectrum harder than the SM one because of the growth with $\sqrt{s}$ associated to the dimension 5 operators in Eq. (1.44). The relative importance of the linear and quadratic terms σ_a and σ_{aa} is illustrated in Fig. 2.3 (right). It can be seen that for large $|\Delta a_t| > 0.1$, the quadratic term σ_{aa} clearly dominates over the interference contribution σ_a. This feature can be understood from the helicity structure of the amplitudes for the Standard Model process and for the anomalous contribution.

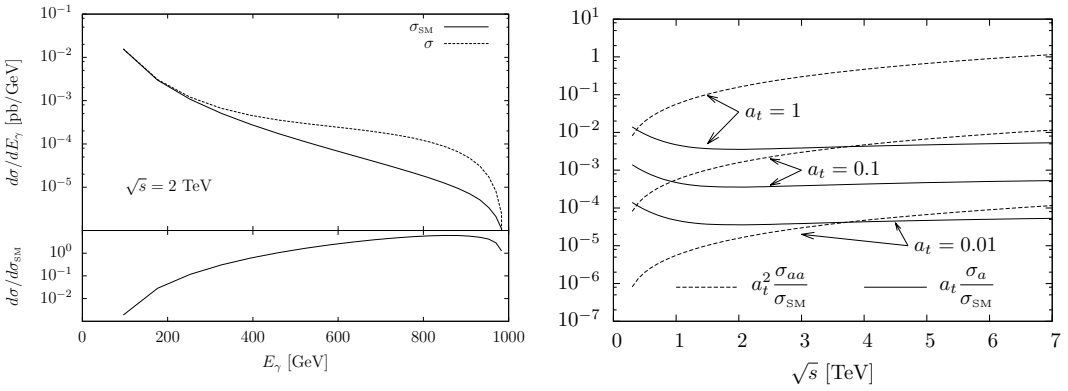

FIGURE 2.3: The parton-level cross section for $ub \to td\gamma$. Left: Photon energy distribution at $\sqrt{s} = 2$ TeV. Standard Model process and anomalous contribution for $\Delta a_t = 1$, $\Delta d_t = 0$. Right: The parton-level cross section as function of the parton-parton centre-of-mass energy $\sqrt{s}$. Ratio of the anomalous terms σ_a and σ_{aa} to the Standard Model process for different values of Δa_t.

Since the dipole moment coupling flips the chirality, see Eq. (1.4), the new interaction in Fig. 2.2 (right) calls for a right-handed top quark in the final state, since the SM charged-current weak interaction that drives the t-channel in single-top production involves left-handed fermions. Small interference can arise only paying another chirality flip through a mass term, that in general is suppressed for $\sqrt{s} \gg m_t$. As a consequence, we expect a bound on Δa_t to be almost insensitive on the sign and limited by quadratic dependence of the cross section on the anomalous coupling. Analogous results are obtained for a non-zero electric dipole moment case when the role of the dimensionless parameter Δa_t is played by $\Delta d_t(2m_t/Q_t e)$ (or even more in general by the complex dipole moment c_f defined in Eq. (1.3)).

2.5 Numerical results for signal and background processes

To assess the potential of single-top-plus-photon production at the LHC (with centre-of-mass energy of 14 TeV), we concentrated on photon radiation in the t-channel single top production process, $pp \to tj\gamma$, followed by $t \to bW^+$, where the W boson decays into an electron or a muon (τ leptons are ignored). We took into account also t-channel single-top production followed by top radiative decay ($t \to bl\nu_l\gamma$). The process is combined with its charge conjugate $pp \to \bar{t}j\gamma$, followed by $\bar{t} \to \bar{b}W^-$. From now on we will refer to these processes simply as "single-top+γ". In the final state of the processes

$$\begin{aligned} pp &\to \gamma l^+ \nu_l b j, \\ pp &\to \gamma l^- \bar{\nu}_l \bar{b} j, \quad \text{with } l = e, \mu, \end{aligned} \tag{2.15}$$

we required two jets, one of them tagged as a b-jet, a hard isolated photon, an isolated lepton and missing energy from the undetected neutrino.

We generated at leading-order parton-level event samples with `MadGraph5` [167]. Besides its Standard Model electromagnetic interaction, the top quark couples with the photon also via the effective operators introduced in Eq. (1.44), by means of a new Madgraph model generated with `FeynRules` [171]. We assumed in general contributions from both the anomalous electric and magnetic dipole moments. In the simulation the top quark mass is $m_t = 173.5$ GeV and all other quarks and leptons masses are set to zero. The single-top cross section is computed in the five-flavour scheme and includes top quark and W decay width effects and full spin correlations. All cross sections for signal and background are computed using CTEQ6L1 parton distribution [172]. The renormalization and factorization scales are chosen event-by-event to be

$$\mu_F^2 = \mu_R^2 = m_t^2 + \sum_i p_T^2(i), \tag{2.16}$$

where m_t is the top mass and the index i runs over the visible particles in the final state.

The acceptance cuts for signal and background events are

$$\begin{gathered} p_T(\gamma) > 100 \text{ GeV}, \quad p_T(j) > 20 \text{ GeV}, \quad p_T(b) > 20 \text{ GeV}, \quad \not{p}_T > 20 \text{ GeV}, \\ |\eta(\gamma)| < 2.5, \quad |\eta(b)| < 2.5, \quad |\eta(j)| < 5, \quad |\eta(l)| < 2.5, \\ \Delta R(j,b) > 0.4, \quad \Delta R(j,l) > 0.4, \quad \Delta R(j,\gamma) > 0.4, \\ \Delta R(l,\gamma) > 0.4, \quad \Delta R(l,b) > 0.4, \quad \Delta R(b,\gamma) > 0.4, \end{gathered} \tag{2.17}$$

where $\Delta R^2 = \Delta\Phi^2 + \Delta\eta^2$ is the separation in the rapidity-azimuth plane and $\not{p}_T$ is the missing momentum due to the undetected neutrino.

The large cut on the photon transverse momentum enhances the contribution from the anomalous couplings, which grow with the photon energy. As a side effect, it also results in a suppression of Standard Model background processes yielding the same final state signature.

In addition to the cuts listed above, we also required the final state to be consistent with the single-top+γ production. In particular to reduce the background, the invariant mass $m(lb\nu)$ of the b-jet, the charged lepton and the neutrino should be close to the top mass. We chose to apply the technique in Ref. [173] for the reconstruction of the unmeasured z-component of the neutrino momentum $p_z(\nu)$. The transverse momentum of the neutrino is given by the x- and y-components of the $\not{E}_T$ vector, while the z-component $p_z(\nu)$ is inferred by imposing a W-boson mass constraint on the lepton-neutrino system. Since the constraint leads to a quadratic equation for $p_z(\nu)$, in case of two real solutions the

smaller one $|p_z|$ is chosen. If the solutions are complex, the neutrino p_x and p_y are rescaled such that the imaginary radical vanishes, but keeps the transverse component of the neutrino as close as possible to $\not{E}_T$. In the end we select events with:

$$150 \text{ GeV} < m(lb\nu) < 200 \text{ GeV}. \tag{2.18}$$

The assumption $m(lb\nu) \sim m_t$ does not take into account the possibility of the radiative top decay where $m_t \sim m(lb\nu\gamma)$. However we checked that the contribution to the total cross section arising from radiative top decay is suppressed by the cut on the photon transverse momentum.

2.5.1 Signal cross section

Imposing the cuts listed in Eqs. (2.17) and (2.18) we obtained a cross sections for single-top-plus-photon production at the $\sqrt{s} = 14$ TeV LHC of 9.0 fb for final states involving a t quark and 5.6 fb for final states involving a $\bar{t}$ quark. In the following, we will always add both these contributions to obtain the single-top-plus-photon production rates.

In Fig. 2.4 we show various distributions for single-top+γ production at the LHC. To illustrate the magnitude of potential effects, we compare the Standard Model prediction with a prediction including a non-standard $tt\gamma$ coupling with $\Delta a_t = 1.0$, $\Delta d_t = 0$. It can be seen that the photon spectrum is considerably harder in the high-p_T region when $\Delta a_t \neq 0$. Consequently, $g-2$ effects are enhanced in the configuration where the top quark (or its decay products b and l) are back to back to the photon, as shown in the ΔR distributions.

2.5.2 Backgrounds

We distinguish two types of backgrounds: the irreducible background from the Standard Model process $pp \to (W \to l\nu_l)bj\gamma$, which yields the identical final state, and potentially reducible backgrounds from various other Standard Model processes that yield different final states that are attributed to the single-top-plus-photon signature due to a misidentification of one or more of the final state objects.

The most important reducible background processes come from light jets faking either a b-jet or photon, or from electrons misidentified as a photons. In the analysis we assumed a b-jet tagging efficiency of $\varepsilon_b = 60\%$ and a corresponding mistag rate of $\varepsilon_{\text{light}} = 0.1\%$ for a light jet (u, d, s quark or gluon) and $\varepsilon_c = 1\%$ for a c-jet, consistent with typical values assumed by the LHC experiments, e.g. [174]. We applied the cuts in Eq. (2.17) where the (mistag) b-jet is chosen randomly.

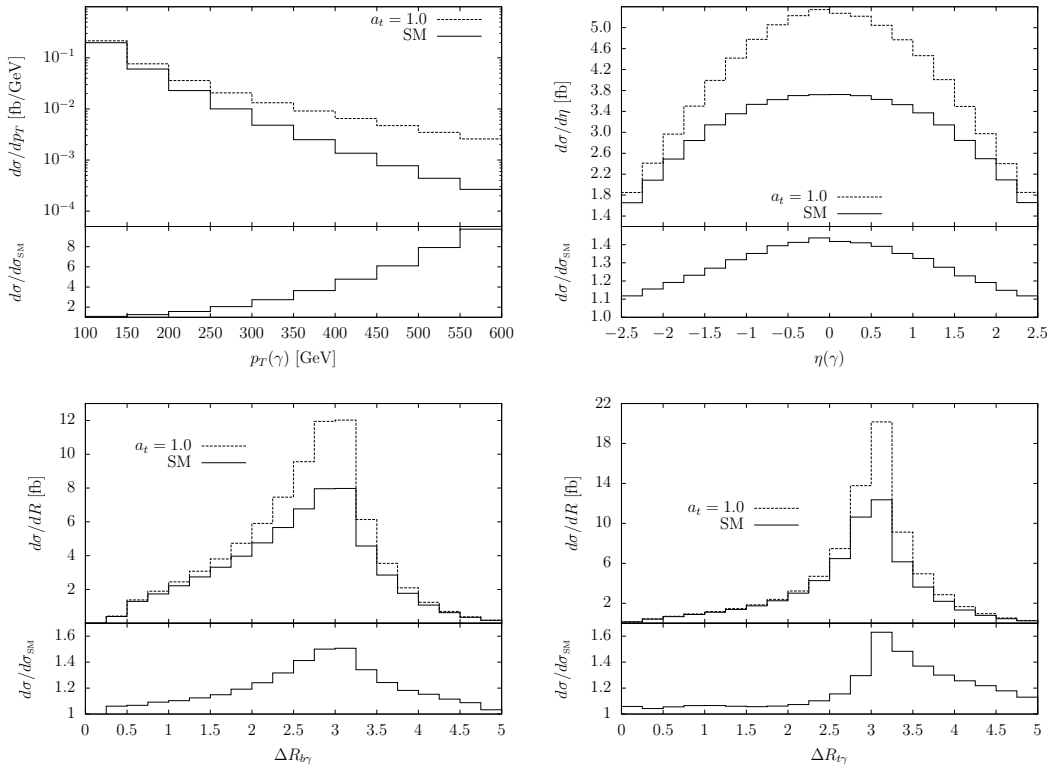

FIGURE 2.4: Kinematical distributions in single-top+γ production at the LHC with $\sqrt{s} = 14$ TeV.

A potentially dangerous background arises from jets misidentified as photons. To estimate the size of these processes we defined a jet fake rate $f_{j\to\gamma}$ as the probability for a light jet to be misidentified as a photon. The rate $f_{j\to\gamma}$ is the one used in the experimental measurement of the $W\gamma$ and $Z\gamma$ cross section and the W+jet cross section at ATLAS [175], which estimated it to be $f_{j\to\gamma} \sim 1/2500$. Similar misidentification rates were reported in the expected performance for the ATLAS detector [176]. Background processes considered are $Wjjj$, $Wbjj$ and $Wbbj$ where a jet with at least $p_T > 100$ GeV fakes a photon (the $Wjjj$ process contributes only if it also yields a mistagged b-jet).

Electrons from W and Z boson decays can be misidentified as photons since the two particles generate similar electromagnetic signatures. The fake rate $f_{e\to\gamma}$, defined as the probability for a true electron to be identified as a converted photon, is estimated thorough the Z boson decay $Z \to ee$ as reported in the measurement of $W\gamma$, $Z\gamma$, $\gamma\gamma$ cross sections [175, 177]. The measured rate varies between 2% and 6% and in our case we conservatively assumed $f_{e\to\gamma} \sim 6\%$. Since we require events with a certain amount of missing energy, the background taken into account here is the full leptonic $t\bar{t}$ production, where the two tops decay $t \to bl^+\nu_l$ and $\bar{t} \to \bar{b}e^-\bar{\nu}_e$. Processes involving a pair of vector bosons, such as $WWjj$ or $WZjj$, turn out to be irrelevant.

Process	Measurable cross section [fb]
s single-top+γ	8.0
$Wbj\gamma$	$\mathcal{O}(10^{-2})$
$t\bar{t}$ full lep.	15.0
$W\gamma$+jets	1.5
W+jets	0.4
$t\bar{t}\gamma$	0.2
$Z\gamma$+jets	$\mathcal{O}(10^{-2})$
Z+jets	$\mathcal{O}(10^{-2})$

TABLE 2.3: Expected cross section for single-top+γ signal and the most important background processes at the LHC. Photon misidentification probabilities and b-jet mistag rates and efficiencies are included.

Other kinds of backgrounds result from Z-bosons decays to leptons, where one lepton is outside the detector coverage ($|\eta_l| > 2.5$) and fakes missing energy. Here we consider $Zbb\gamma$, $Zbj\gamma$, $Zjj\gamma$ and $t\bar{t}\gamma$. All these kinds of processes are negligible in our case.

Table 2.3 summarises the (Standard Model, without anomalous couplings) signal and background cross sections after the application of the cuts in Eqs. (2.17) and (2.18). For the single-top+γ cross section the b-tagging efficiency is included, thereby lowering the total cross section from the parton-level value stated above.

We observe that the signal process is two orders of magnitude larger than the irreducible background, and half the sum of all reducible background processes. It is clear that it will be possible to establish the Standard Model single-top-plus-photon process in the region of high photon-p_T already with moderate luminosity. However, a detection of anomalous couplings in this process requires a precision measurement of the cross section and of differential distributions. In the following, we use our simulation to determine the sensitivity of future LHC measurements of single-top-plus-photon process on a potential anomalous magnetic moment of the top quark.

2.6 Bounds from future LHC data

We used the shape of the photon transverse momentum distribution to derive quantitative sensitivity bounds that can be obtained on the anomalous dipole moments of the top quark. After imposing the cuts in Eqs. (2.17) and (2.18), we combined channels with electrons and muons in the final state. We performed a χ^2 test on the distributions

and calculated 68.3% and 95% confidence level limits. We used the χ^2 expression of [9],

$$\chi^2 = \sum_{i=1}^{n_D} \frac{N_i - f N_i^{\rm SM}}{f N_i^{\rm SM}}, \tag{2.19}$$

where n_D if the number of histogram bins, $N_i^{\rm SM}$ is the number events expected in the SM, N_i is the number of events for a given set $(\Delta a_t, \Delta d_t)$ of anomalous couplings. The parameter f reflects the uncertainty in the SM cross section normalization within the allowed range and it is determined minimizing the χ^2 [9]:

$$f = \begin{cases} (1+\Delta\mathcal{N})^{-1}, & \text{for } \bar{f} < (1+\Delta\mathcal{N})^{-1}, \\ \bar{f}, & \text{for } (1+\Delta\mathcal{N})^{-1} < \bar{f} < (1+\Delta\mathcal{N}), \\ (1+\Delta\mathcal{N}), & \text{for } \bar{f} > (1+\Delta\mathcal{N}), \end{cases} \tag{2.20}$$

with

$$\bar{f}^2 = \sum_{i=1}^{n_D} \frac{N_i^2}{N_i^{\rm SM}} \left[\sum_{i=1}^{n_D} N_i^{\rm SM} \right]^{-1}. \tag{2.21}$$

The parameter $\Delta\mathcal{N}$ is the SM cross section normalization uncertainty. In analogy with [9] we chose $\Delta\mathcal{N} = 30\%$. Throughout the calculation, we noted that $\bar{f}$ is usually very close to unity, so that the cross section normalization plays a small role in the sensitivity.

The dominant backgrounds consist of $t\bar{t}$, $W\gamma$+jets and W+jets. Other sources of background are neglected. Limits at the LHC, with $\sqrt{s} = 14$ TeV are computed for an integrated luminosity of 30 fb^{-1} (one year of operation), 300 fb^{-1} (integrated luminosity expected from the upcoming run period) and 3000 fb^{-1} (high-luminosity upgrade option). The sensitivity bounds are shown in Fig. 2.5 and Tab. 2.4. As already discussed in Section 2.4 above, the measurement is insensitive on the sign of the anomalous dipole moments and on the interplay of Δa_t and Δd_t due to the dominance of the self-interference term.

coupling	30 fb^{-1}	300 fb^{-1}	3000 fb^{-1}
Δa_t	$^{+0.94}_{-0.92}$	$^{+0.39}_{-0.38}$	$^{+0.22}_{-0.21}$
$\Delta d_t\,[10^{-17} e{\cdot}\text{cm}]$	$^{+3.5}_{-3.4}$	$^{+1.5}_{-1.5}$	$^{+0.83}_{-0.82}$

TABLE 2.4: Sensitivity achievable at 95% C.L. in single-top+γ at the LHC ($\sqrt{s} = 14$ TeV) for an integrated luminosities of 30 fb^{-1}, 300 fb^{-1} and 3000 fb^{-1}.

Concentrating on the limits at 95% confidence level, we observe that with 30 fb^{-1} only contributions to the dipole moments at order unity could be detected. With higher luminosity, these limits improve towards 0.4 (at 300 fb^{-1}) and 0.2 (at 3000 fb^{-1}). Compared

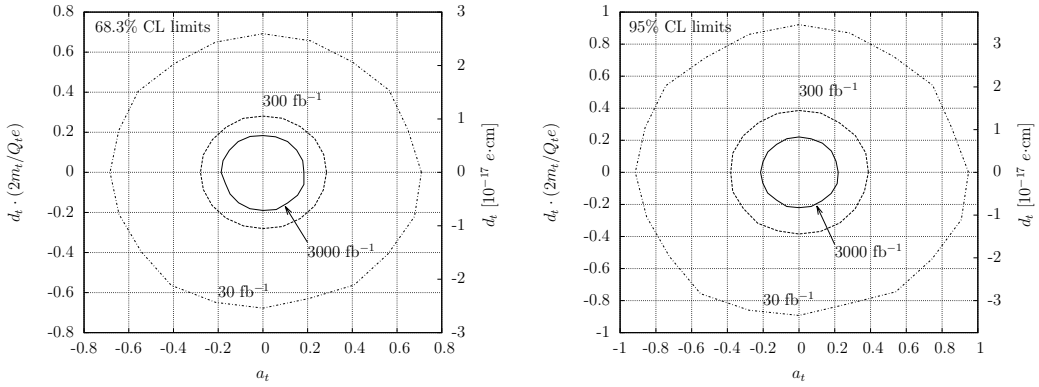

FIGURE 2.5: Bounds on the anomalous dipole moments of the top quark at 68% (left) and 95% (right) confidence level, for LHC operation at $\sqrt{s} = 14$ TeV.

with the current bounds (2.6), which arise essentially from flavour physics observables and are thus of indirect nature, a significant improvement can be obtained. Depending on the sign of Δa_t or Δd_t, the improved constraints with a luminosity of 3000 fb^{-1} can be up to a factor 10 more restrictive than current bounds.

	single-top+γ $\mathcal{L} = 300$ fb^{-1}	$t\bar{t}\gamma$ [9] $\mathcal{L} = 300$ fb^{-1}
$\Delta F_{2V}^{\gamma} = Q_t \Delta a_t$	$^{+0.22}_{-0.21}$	$^{+0.19}_{-0.20}$
$\Delta F_{2A}^{\gamma} = \Delta d_t (2m_t)/e$	$^{+0.21}_{-0.21}$	$^{+0.19}_{-0.21}$

TABLE 2.5: Sensitivities achievable at 68.3% C.L. for anomalous $tt\gamma$ couplings at LHC, expected from the upcoming run period $\mathcal{L} = 300$ fb^{-1}, in single-top+γ production and $t\bar{t}\gamma$ production (in the semileptonic channel $pp \to t\bar{t}\gamma \to \gamma l\nu b\bar{b}jj$) [9]. Here bounds are expressed in terms of vertex form factors $\Delta F_{2V}^{\gamma}, \Delta F_{2A}^{\gamma}$ as in [9].

In [9], anticipated limits (for the same luminosity scenarios) from $t\bar{t}\gamma$ final states on the anomalous interactions of the top quarks were expressed in terms of the form factors $F_{2V}(0)$ and $F_{2A}(0)$ defined in Eq. (1.2). These limits can be converted in a straightforward manner into limits on the anomalous dipole moments considered here. The limits at 95% confidence level that are obtained by $t\bar{t}\gamma$ production are very similar to those obtained here from single-top-plus-photon production. Both channels are completely independent from each other, and a combination of them could thus further improve the sensitivity.

Conclusions

We investigated the possibility to measure the anomalous magnetic moment and the electric dipole moment of the top quark, in single-top-plus-photon production at the LHC, and tau lepton, in radiative leptonic tau decays at the future Belle II experiment.

Several proposals to determine the dipole moments of these particles are based on a precise measurement of processes where an isolated photon is emitted in the production or the decay. The $tt\gamma$ coupling may be measured at the LHC via analysis of direct production of $t\bar{t}$ pairs or single-top in association with a photon. Their extraction in top quark pair production from $t\bar{t}\gamma$ final states was studied in detail in Ref. [9]. In the case of the tau lepton, the well-known method suggested in [16] promises a sensitivity down to 10^{-5}, but it suffers from the issue that at Belle and Belle II experiments the resonant $e^+e^- \to \Upsilon \to \tau^+\tau^-$ events cannot be separated from non-resonant ones.

For this reason we advocated the alternative measurement of the tau lepton dipole moments via its radiative decays. The possibility to measure the $g-2$ of the tau taking advantage of the phenomenon of radiation zero in tau radiative decays has already been proposed in [72]. However we have shown that this method has essentially no chance to detect not even a value of $a_\tau \sim 1$ at Belle. We therefore adopted a more comprehensive and most powerful method to extract $\tilde{a}_\tau$ and $\tilde{d}_\tau$: an unbinned maximum likelihood fit of events in the full phase space. The desired sensitivity, $\mathcal{O}(10^{-3})$, required an analogous precision on the theoretical side. For this reason, we included in the decay rate prediction NLO QED corrections and W-boson propagator effects. Also, we observed some discrepancies between our result and that of Ref. [112]. The obtained prediction for the $\tau \to l\nu\bar{\nu}\gamma$ differential decay rate was used in a dedicated feasibility study, where the whole data sample collected at Belle has been analyzed together with that planned in the Belle II experiment. Dipole moments effects, included via an effective Lagrangian, slightly modify the shapes of the kinematical distributions. We showed that the sensitivity to the anomalous magnetic moment at Belle II, $\tilde{a}_\tau \sim 0.012$, can be already competitive with the current bound from the DELPHI experiment, while the expected

sensitivity to the tau EDM, $\tilde{d}_\tau \sim 0.011$, is still worse than the most precise measurement done at Belle.

Our initial expectation was to reach a precision of $\mathcal{O}(10^{-3})$, i.e the same order of magnitude of the tau $g-2$. However, it was difficult to estimate the sensitivity in this multidimensional likelihood fit before performing it. Here the question was how strong are the peculiarities of the multidimensional shape associated with the additional $\tilde{a}_\tau$ and $\tilde{d}_\tau$ terms. Indeed, the functions G_a, G_d, J_a etc., are suppressed in comparison with G, J, K: at small y-values $G \sim 1/y^2$ but $G_a \sim 1$ ($y = 2E_\gamma/m_\tau$). So the final sensitivity is determined by the interplay between peculiarities of the dipole-moment related shapes, which tend to increase the sensitivity, and the mentioned suppression, which tends to decrease it. Eventually, the issue could be solved only in our real feasibility study. The possibility to reconsider and ameliorate these results will be taken into account when the collider will be operating and properly tuned. Also, the extraction of $\tilde{a}_\tau$ and $\tilde{d}_\tau$ from the $\tau\tau$ production vertex, i.e. from the analysis of $e^+e^- \to \tau^+\tau^-$ events where the statistics is huge, is definitely not excluded, but a careful theoretical reanalysis of [16] is needed.

In this thesis, we have also extended the analysis of $t\bar{t}\gamma$ final states in [9] to single-top quark production processes at the LHC and demonstrated the sensitivity of single-top-plus-photon production to the anomalous dipole moments of the top quark. We have shown that the contributions from the corresponding effective operators yield a photon transverse momentum spectrum harder than what is expected in the Standard Model. By simulating the signal process and all potentially relevant irreducible and reducible backgrounds to it, we have quantified the numerical magnitude of anomalous top quark dipole moments that could be detected in the 14 TeV runs at the LHC with different luminosity scenarios. Our results are summarised in Fig. 2.5, they demonstrate that the bounds that can be obtained from single-top-plus-photon production, of $\mathcal{O}(20\% - 30\%)$, are very much comparable in magnitude to those that can be obtained from $t\bar{t}\gamma$ final states [9], and a combination of the two processes can potentially ameliorate existing bounds [14, 15] by up to an order of magnitude.

The determination of $tt\gamma$ couplings can be further improved at future linear colliders by exploiting the $t\bar{t}$ final state correlations [10]. In various scenario of e^+e^- colliders with $\sqrt{s} > 2m_t$ it has been shown that the top quark precision physics can receive a powerful boost. Concerning the sensitivity for anomalous coupling, they are expected to be improved by more that an order of magnitude with respect to the LHC potential. In particular, there is the actual possibility to test Δa_t and Δd_t at the level of 10^{-2}-10^{-3} [178–180].

Appendix
Radiative leptonic decay formulas

The differential decay rate for $\tau \to \nu_\tau \bar{\nu}_\ell \ell \gamma$ is

$$\begin{aligned}\frac{d^6\,\Gamma}{dx\,dy\,d\Omega_\ell\,d\Omega_\gamma} &= \frac{\alpha\, m_\tau^5 G_F^2}{(4\pi)^8}\,\frac{xy\beta}{1+\delta_W(m_\mu,m_e)}\Big\{G(x,y,z) + x\beta\,\hat{n}\cdot\hat{p}_\ell\,J(x,y,z) \\ &\quad + y\,\hat{n}\cdot\hat{p}_\gamma\,K(x,y,z) + xy\beta\,\hat{p}_\ell\cdot(\hat{p}_\gamma\times\hat{n})\,L(x,y,z)\Big\}\,,\end{aligned} \tag{22}$$

with $r = m_\ell/m_\tau$, $\beta = \sqrt{1-4r^2/x^2}$, $z = xy(1-c\,\beta)$ and where $\hat{n}$ is the unit vector in the direction of the tau polarization. The functions G, J and K get a tree-level, a one-loop, a W-propagator, an $\tilde{a}_\tau$ and a $\tilde{d}_\tau$ contribution, while L is generated only by the effective operators. Their expressions are

$$\begin{aligned}G(x,y,z) &= G_{\rm LO} + \frac{\alpha}{\pi}\,G_{\rm NLO} + r_W^2 G_W + {\rm Re}(\tilde{a}_\tau)G_a + {\rm Im}(\tilde{d}_\tau)G_d\,,\\ J(x,y,z) &= J_{\rm LO} + \frac{\alpha}{\pi}\,J_{\rm NLO} + r_W^2 J_W + {\rm Re}(\tilde{a}_\tau)J_a + {\rm Im}(\tilde{d}_\tau)J_d\,,\\ K(x,y,z) &= K_{\rm LO} + \frac{\alpha}{\pi}\,K_{\rm NLO} + r_W^2 K_W + {\rm Re}(\tilde{a}_\tau)K_a + {\rm Im}(\tilde{d}_\tau)K_d\,,\\ L(x,y,z) &= {\rm Im}(\tilde{a}_\tau)L_a + {\rm Re}(\tilde{d}_\tau)L_d\,,\end{aligned} \tag{23}$$

with $r_W = m_\tau/M_W$. Higher orders terms in r_W, $\tilde{a}_\tau$ and $\tilde{d}_\tau$ can be neglected. NLO corrections can be obtained in a Fortran code from the author. The above functions take the following form:

$$
\begin{aligned}
G_{\mathrm{LO}} = -\frac{64\pi^2}{3y^2z^2}\big[\, & r^4\left(6xy^2+6y^3-6y^2z-8y^2\right)+r^2\left(-4x^2y^2-6x^2yz-8xy^3+2xy^2z\right.\\
& +6xy^2+6xyz^2+8xyz+6xz^2-4y^4+5y^3z+6y^3-2y^2z^2-6y^2z-3yz^3+6yz^2\\
& \left.-6z^3-8z^2\right)+4x^3yz+8x^2y^2z-8x^2yz^2-6x^2yz-4x^2z^2+6xy^3z-8xy^2z^2-6xy^2z\\
& +6xyz^3-2xyz^2+8xz^3+6xz^2+2y^4z-2y^3z^2-3y^3z+2y^2z^3-2y^2z^2-2yz^4\\
& +5yz^3+6yz^2-4z^4-6z^3\big] \qquad (24)
\end{aligned}
$$

$$
\begin{aligned}
J_{\mathrm{LO}} = -\frac{64\pi^2}{3y^2z^2}\big\{ & 6r^4y^2+r^2\left[y^2(-4x+z+2)+3yz(z-2x)-4y^3+6z^2\right]\\
& +z\left[4x^2y+x\left(6y^2-2y(3z+1)-4z\right)+2y^3-y^2(4z+1)+yz(2z-3)+2z(2z+1)\right]\big\}
\end{aligned} \qquad (25)
$$

$$
\begin{aligned}
K_{\mathrm{LO}} = -\frac{64\pi^2}{3y^2z^2}\big\{ & 6r^4y(y-z)+r^2\left[y^2(-4x+5z+2)+yz(x-2(z+1))+3z^2(x-z)-4y^3\right]\\
& -z\left[-2x^2(y-z)+x\left(-4y^2+4yz+y-z(4z+1)\right)-2y^3+y^2(2z+1)\right.\\
& \left.-2y(z-1)z+z^2(2z+1)\right]\big\} \qquad (26)
\end{aligned}
$$

$$
G_a = \frac{64\pi^2}{3yz}\Big\{r^2\left(y^2-zy+3z^2\right)-(x+y-z-1)z(y+2z)\Big\}\,, \qquad (27)
$$

$$
\begin{aligned}
G_d = & -\frac{128\pi^2}{3y^2z}\Big\{6y^2r^4+\left(-3y^3+(-4x+z+2)y^2+3z(z-2x)y+6z^2\right)r^2\\
& +z\left(y^3-(3z+1)y^2+4x^2y+2(z-1)zy+2z(2z+1)\right.\\
& \left.+x\left(5y^2-2(3z+1)y-4z\right)\right)\Big\}\,, \qquad (28)
\end{aligned}
$$

$$
\begin{aligned}
J_a = & -\frac{64\pi^2}{3yz}\Big\{-2y^3+\left(3r^2+2z+2\right)y^2-2x^2y+3zy-2z\left(3r^2+2z+1\right)\\
& +x\left(3yr^2-4y^2+y+2yz+4z\right)\Big\}\,, \qquad (29)
\end{aligned}
$$

$$
J_d = \frac{128\pi^2}{3z}\Big\{(-3x-3y+4)r^2+2x^2+2y^2-2y+x(4y-2z-3)-2yz+z\Big\}\,, \qquad (30)
$$

$$K_a = \frac{64\pi^2}{3y^2z}\Big\{ -12yr^4 + \big(3(x+2)y^2 + \big(3x^2+8x-8z-4\big)y - 6z^2\big)r^2 - 2x^3y + x^2y(-4y+2z+1) - 2z\left(-y^2-zy+y+2z^2+z\right) + x\left(-2y^3+2(z+1)y^2 + zy + 4z^2\right)\Big\}, \tag{31}$$

$$K_d = \frac{128\pi^2}{3y^2z}\Big\{ -2yx^3 + \big(-4y^2+(2z+3)y+4z\big)x^2 + \big(-2y^3+2(z+1)y^2+5zy - 2z(4z+3)\big)x + r^2\left(3yx^2+3y^2x-4yx-6zx+2y^2+6z^2-8yz+8z\right) + 2z\left(y^2-(3z+1)y+z(2z+3)\right)\Big\}, \tag{32}$$

$$L_a = -\frac{32\pi^2}{3yz}\Big\{(-3x-3y+4)r^2 + 2x^2+2y^2-2y+x(4y-2z-3)-2yz+z\Big\}, \tag{33}$$

$$L_d = \frac{64\pi^2}{3y^2z}\Big\{2y^3 - \left(3r^2+2z+2\right)y^2 + 2x^2y - 3zy + 2z\left(3r^2+2z+1\right) + x\left(4y^2 - \left(3r^2+2z+1\right)y - 4z\right)\Big\}. \tag{34}$$

$$G_W = \frac{64\pi^2}{3y^2z^2}\Big\{4r^6y^2 - 2r^4\left(2x^2y^2+4xy^3-4xy^2z-2xy^2+2xyz+2y^4-7y^3z-2y^3 + 2y^2z^2+2y^2z-2y^2-2z^2\right) + r^2\left(2x^3y^2+4x^3yz+6x^2y^3+2x^2y^2z-4x^2y^2-8x^2yz^2 - 4x^2yz-4x^2z^2+6xy^4-12xy^3z-8xy^3-8xy^2z^2+4xy^2z+6xyz^3-4xyz^2-4xyz + 8xz^3+4xz^2+2y^5-9y^4z-4y^4+4y^3z^2+12y^3z+5y^2z^3-4y^2z^2-2yz^4+12yz^3 + 4yz^2-4z^4-4z^3+4z^2\right) - z\left(2x^4y+6x^3y^2-6x^3yz-4x^3y-2x^3z+7x^2y^3-6xy^3 - 16x^2y^2z-8x^2y^2+7x^2yz^2+2x^2yz+6x^2z^2+4x^2z+4xy^4-14xy^3z+14xy^2z^2 + 8xy^2z-4xyz^3+12xyz^2+8xyz-6xz^3-8xz^2+y^5-4y^4z-2y^4+6y^3z^2+5y^3z - 4y^2z^3+4y^2z^2+4y^2z+yz^4-9yz^3-14yz^2+2z^4+4z^3\right)\Big\}, \tag{35}$$

$$J_W = \frac{32\pi^2}{3y^2z^2}\Big\{ -8r^4y^2(x+y-z) + r^2\left(4x^2y^2+8x^2yz+8xy^3+4xy^2z-12xyz^2-8xz^2 + 4y^4-5y^3z-8y^2z^2+4yz^3-8yz^2+8z^3\right) + z\left(-4x^3y-10x^2y^2+10x^2yz+4x^2z - 8xy^3+21xy^2z-8xyz^2+8xyz-8xz^2-y^4+10y^3z-y^3-11y^2z^2 + 2y^2z+2yz^3-10yz^2+4z^3\right)\Big\}, \tag{36}$$

$$K_W = \frac{32\pi^2}{3y^2z^2}\Big\{ -4r^4y\left(2xy-2xz+2y^2-7yz+2z^2\right)+r^2\left(4x^2y^2-4x^2z^2+8xy^3\right.$$
$$-19xy^2z-8xyz^2+8xz^3+4y^4-18y^3z+8y^2z^2+8y^2z+10yz^3+6yz^2-4z^4\big)$$
$$-z\left(2x^3y-2x^3z+6x^2y^2-11x^2yz+6x^2z^2+7xy^3-18xy^2z-xy^2+17xyz^2+2xyz\right.$$
$$\left.-6xz^3+2y^4-8y^3z+12y^2z^2-8yz^3-2yz+2z^4\right)\Big\} \qquad (37)$$

Bibliography

[1] D. Hanneke, S. Fogwell, and G. Gabrielse, "New Measurement of the Electron Magnetic Moment and the Fine Structure Constant," Phys.Rev.Lett. **100**, 120801 (2008), 0801.1134.

[2] G. Bennett et al. (Muon G-2 Collaboration), "Final Report of the Muon E821 Anomalous Magnetic Moment Measurement at BNL," Phys.Rev. **D73**, 072003 (2006), hep-ex/0602035.

[3] G. Giudice, P. Paradisi, and M. Passera, "Testing new physics with the electron g-2," JHEP **1211**, 113 (2012), 1208.6583.

[4] A. Czarnecki and W. J. Marciano, "Electromagnetic dipole moments and new physics," (2010).

[5] H. Murayama and M. E. Peskin, "Physics opportunities of e^+e^- linear colliders," Ann.Rev.Nucl.Part.Sci. **46**, 533 (1996), hep-ex/9606003.

[6] C. T. Hill and E. H. Simmons, "Strong dynamics and electroweak symmetry breaking," Phys.Rept. **381**, 235 (2003), hep-ph/0203079.

[7] M. Pospelov and A. Ritz, in *Lepton dipole moments*, edited by B. Roberts (World Scientific, 2010), Advanced Series on Directions in High Energy Physics n. 20.

[8] L. Mercolli and C. Smith, "EDM constraints on flavored CP-violating phases," Nucl.Phys. **B817**, 1 (2009), 0902.1949.

[9] U. Baur, A. Juste, L. Orr, and D. Rainwater, "Probing electroweak top quark couplings at hadron colliders," Phys.Rev. **D71**, 054013 (2005), hep-ph/0412021.

[10] B. Grzadkowski and Z. Hioki, "Optimal observable analysis of the angular and energy distributions for top quark decay products at polarized linear colliders," Nucl.Phys. **B585**, 3 (2000), hep-ph/0004223.

[11] G. Altarelli, R. Barbieri, and S. Jadach, "Toward a model independent analysis of electroweak data," Nucl.Phys. **B369**, 3 (1992).

[12] G. Altarelli, R. Barbieri, and F. Caravaglios, "Nonstandard analysis of electroweak precision data," Nucl.Phys. **B405**, 3 (1993).

[13] O. J. Eboli, M. Gonzalez-Garcia, and S. Novaes, "Limits on anomalous top couplings from Z pole physics," Phys.Lett. **B415**, 75 (1997), hep-ph/9704400.

[14] J. F. Kamenik, M. Papucci, and A. Weiler, "Constraining the dipole moments of the top quark," Phys.Rev. **D85**, 071501 (2012), 1107.3143.

[15] A. O. Bouzas and F. Larios, "Electromagnetic dipole moments of the Top quark," Phys.Rev. **D87**, 074015 (2013), 1212.6575.

[16] J. Bernabeu, G. Gonzalez-Sprinberg, J. Papavassiliou, and J. Vidal, "Tau anomalous magnetic moment form-factor at super B/flavor factories," Nucl.Phys. **B790**, 160 (2008), 0707.2496.

[17] J. Abdallah et al. (DELPHI Collaboration), "Study of tau-pair production in photon-photon collisions at LEP and limits on the anomalous electromagnetic moments of the tau lepton," Eur.Phys.J. **C35**, 159 (2004), hep-ex/0406010.

[18] S. Eidelman and M. Passera, "Theory of the tau lepton anomalous magnetic moment," Mod.Phys.Lett. **A22**, 159 (2007), hep-ph/0701260.

[19] K. Inami et al. (Belle Collaboration), "Search for the electric dipole moment of the tau lepton," Phys.Lett. **B551**, 16 (2003), hep-ex/0210066.

[20] R. Bonciani, P. Mastrolia, and E. Remiddi, "QED vertex form-factors at two loops," Nucl.Phys. **B676**, 399 (2004), hep-ph/0307295.

[21] P. Mastrolia and E. Remiddi, "Two loop form-factors in QED," Nucl.Phys. **B664**, 341 (2003), hep-ph/0302162.

[22] S. M. Barr and W. J. Marciano, "Electric dipole moments," Adv.Ser.Direct.High Energy Phys. **3**, 455 (1989).

[23] I. Khriplovich and S. Lamoreaux, *CP violation without strangeness: Electric dipole moments of particles, atoms, and molecules* (Springer, 1997).

[24] E. D. Commins, "Electric dipole moments of elementary particles, nuclei, atoms, and molecules," J.Phys.Soc.Jap. **76**, 111010 (2007).

[25] B. L. Roberts and W. J. Marciano, *Lepton dipole moments*, Advanced Series on Directions in High Energy Physics n.20 (World Scientific, 2010).

[26] P. J. Mohr and B. N. Taylor, "CODATA recommended values of the fundamental physical constants: 2002," Rev.Mod.Phys. **77**, 1 (2005).

[27] K. Hagiwara et al. (Particle Data Group), "Review of particle physics. Particle Data Group," Phys.Rev. **D66**, 010001 (2002).

[28] T. Kinoshita and W. J. Marciano, *Quantum Electrodynamics* (World Scientific, 1990).

[29] J. S. Schwinger, "On Quantum electrodynamics and the magnetic moment of the electron," Phys.Rev. **73**, 416 (1948).

[30] C. M. Sommerfield, "Magnetic Dipole Moment of the Electron," Phys.Rev. **107**, 328 (1957).

[31] H. Elend, "On the anomalous magnetic moment of the muon," Physics Letters **20**, 682 (1966).

[32] M. Passera, "The Standard model prediction of the muon anomalous magnetic moment," J.Phys. **G31**, R75 (2005), hep-ph/0411168.

[33] M. Passera, "Precise mass-dependent QED contributions to leptonic g-2 at order α^2 and α^3," Phys.Rev. **D75**, 013002 (2007), hep-ph/0606174.

[34] S. Laporta and E. Remiddi, "The Analytical value of the electron (g-2) at order α^3 in QED," Phys.Lett. **B379**, 283 (1996), hep-ph/9602417.

[35] K. Nakamura et al. (Particle Data Group), "Review of particle physics," J.Phys. **G37**, 075021 (2010).

[36] R. Jackiw and S. Weinberg, "Weak interaction corrections to the muon magnetic moment and to muonic atom energy levels," Phys.Rev. **D5**, 2396 (1972).

[37] I. Bars and M. Yoshimura, "Muon magnetic moment in a finite theory of weak and electromagnetic interaction," Phys.Rev. **D6**, 374 (1972).

[38] G. Altarelli, N. Cabibbo, and L. Maiani, "The Drell-Hearn sum rule and the lepton magnetic moment in the Weinberg model of weak and electromagnetic interactions," Phys.Lett. **B40**, 415 (1972).

[39] W. A. Bardeen, R. Gastmans, and B. Lautrup, "Static quantities in Weinberg's model of weak and electromagnetic interactions," Nucl.Phys. **B46**, 319 (1972).

[40] K. Fujikawa, B. Lee, and A. Sanda, "Generalized Renormalizable Gauge Formulation of Spontaneously Broken Gauge Theories," Phys.Rev. **D6**, 2923 (1972).

[41] A. Czarnecki, B. Krause, and W. J. Marciano, "Electroweak Fermion loop contributions to the muon anomalous magnetic moment," Phys.Rev. **D52**, 2619 (1995), hep-ph/9506256.

[42] A. Czarnecki, B. Krause, and W. J. Marciano, "Electroweak corrections to the muon anomalous magnetic moment," Phys.Rev.Lett. **76**, 3267 (1996), hep-ph/9512369.

[43] G. Degrassi and G. Giudice, "QED logarithms in the electroweak corrections to the muon anomalous magnetic moment," Phys.Rev. **D58**, 053007 (1998), hep-ph/9803384.

[44] L. Bouchait and L. Michel, "La résonance dans la diffusion méson pi- méson pi et le moment magnétique anormal du méson mu," J. Phys. Radium (1961).

[45] L. Durand, "Pionic Contributions to the Magnetic Moment of the Muon," Phys.Rev. **128**, 441 (1962).

[46] S. J. Brodsky and E. De Rafael, "Suggested boson - lepton pair couplings and the anomalous magnetic moment of the muon," Phys.Rev. **168**, 1620 (1968).

[47] M. Gourdin and E. De Rafael, "Hadronic contributions to the muon g-factor," Nucl.Phys. **B10**, 667 (1969).

[48] B. Krause, "Higher order hadronic contributions to the anomalous magnetic moment of leptons," Phys.Lett. **B390**, 392 (1997), hep-ph/9607259.

[49] C. Jarlskog, "A Basis Independent Formulation of the Connection Between Quark Mass Matrices, CP Violation and Experiment," Z.Phys. **C29**, 491 (1985).

[50] C. Jarlskog, "Commutator of the Quark Mass Matrices in the Standard Electroweak Model and a Measure of Maximal CP Violation," Phys.Rev.Lett. **55**, 1039 (1985).

[51] L.-L. Chau and W.-Y. Keung, "Comments on the Parametrization of the Kobayashi-Maskawa Matrix," Phys.Rev.Lett. **53**, 1802 (1984).

[52] M. Kobayashi and T. Maskawa, "CP Violation in the Renormalizable Theory of Weak Interaction," Prog.Theor.Phys. **49**, 652 (1973).

[53] F. Hoogeveen, "The Standard Model Prediction for the Electric Dipole Moment of the Electron," Nucl.Phys. **B341**, 322 (1990).

[54] M. Pospelov and I. Khriplovich, "Electric dipole moment of the W boson and the electron in the Kobayashi-Maskawa model," Sov.J.Nucl.Phys. **53**, 638 (1991).

[55] E. Commins, "Electric dipole moments of leptons," Adv.At.Mol.Opt.Phys. **40**, 1 (1999).

[56] J. Hudson, D. Kara, I. Smallman, B. Sauer, M. Tarbutt, et al., "Improved measurement of the shape of the electron," Nature **473**, 493 (2011).

[57] T. Fukuyama, "Searching for New Physics beyond the Standard Model in Electric Dipole Moment," Int.J.Mod.Phys. **A27**, 1230015 (2012), 1201.4252.

[58] W. Bernreuther, O. Nachtmann, and P. Overmann, "The CP violating electric and weak dipole moments of the tau lepton from threshold to 500-GeV," Phys.Rev. **D48**, 78 (1993).

[59] F. Cornet and J. I. Illana, "Tau pair production via photon-photon collisions at LEP," Phys.Rev. **D53**, 1181 (1996), hep-ph/9503466.

[60] G. A. Gonzalez-Sprinberg, A. Santamaria, and J. Vidal, "Model independent bounds on the tau lepton electromagnetic and weak magnetic moments," Nucl.Phys. **B582**, 3 (2000), hep-ph/0002203.

[61] F. del Aguila, F. Cornet, and J. I. Illana, "The Possibility of using a large heavy ion collider for measuring the electromagnetic properties of the tau-lepton," Phys.Lett. **B271**, 256 (1991).

[62] M. A. Samuel and G. Li, "Measuring the magnetic moment of the tau lepton at the Fermilab tevatron, the, SSC and the LHC," Int.J.Theor.Phys. **33**, 1471 (1994).

[63] I. J. Kim, "Magnetic Moment Measurement of Baryons With Heavy Flavored Quarks by Planar Channeling Through Bent Crystal," Nucl.Phys. **B229**, 251 (1983).

[64] D. Chen et al. (E761 Collaboration), "First observation of magnetic moment precession of channeled particles in bent crystals," Phys.Rev.Lett. **69**, 3286 (1992).

[65] M. A. Samuel, G.-w. Li, and R. Mendel, "The Anomalous magnetic moment of the tau lepton," Phys.Rev.Lett. **67**, 668 (1991).

[66] K. Ikado et al. (Belle Collaboration), "Evidence of the Purely Leptonic Decay B -¿ tau- anti-nu(tau)," Phys.Rev.Lett. **97**, 251802 (2006), hep-ex/0604018.

[67] T. Aushev, W. Bartel, A. Bondar, J. Brodzicka, T. Browder, et al., "Physics at Super B Factory," (2010), 1002.5012.

[68] Y. Ohnishi, T. Abe, T. Adachi, K. Akai, Y. Arimoto, et al., "Accelerator design at SuperKEKB," PTEP **2013**, 03A011 (2013).

[69] S. Banerjee, B. Pietrzyk, J. M. Roney, and Z. Was, "Tau and muon pair production cross-sections in electron-positron annihilations at $\sqrt{s} = 10.58$ GeV," Phys.Rev. **D77**, 054012 (2008), 0706.3235.

[70] H. Koiso, A. Morita, Y. Ohnishi, K. Oide, and K. Satoh, "Lattice of the KEKB colliding rings," Prog. Theor. Exp. Phys. **2013**, 03A009 (2013).

[71] A. Artamonov, S. Baru, A. Blinov, A. Bondar, A. Bukin, et al., "A High Precision Measurement of the Υ, Υ' and Υ'-prime Meson Masses," Phys.Lett. **B137**, 272 (1984).

[72] M. Laursen, M. A. Samuel, and A. Sen, "Radiation Zeros and a Test for the g Value of the τ Lepton," Phys.Rev. **D29**, 2652 (1984).

[73] W. Buchmuller and D. Wyler, "Effective Lagrangian Analysis of New Interactions and Flavor Conservation," Nucl.Phys. **B268**, 621 (1986).

[74] C. N. Leung, S. Love, and S. Rao, "Low-Energy Manifestations of a New Interaction Scale: Operator Analysis," Z.Phys. **C31**, 433 (1986).

[75] M. S. Bilenky and A. Santamaria, "One loop effective Lagrangian for a standard model with a heavy charged scalar singlet," Nucl.Phys. **B420**, 47 (1994), hep-ph/9310302.

[76] M. Fael, L. Mercolli, and M. Passera, "W-propagator corrections to muon and tau leptonic decays," Phys.Rev. **D88**, 093011 (2013), 1310.1081.

[77] A. Ferroglia, C. Greub, A. Sirlin, and Z. Zhang, "Contributions of the W-boson propagator to muon and tau leptonic decay rates," Phys.Rev. **D88**, 033012 (2013), 1307.6900.

[78] A. Sirlin, "Radiative Corrections in the SU(2)-L x U(1) Theory: A Simple Renormalization Framework," Phys.Rev. **D22**, 971 (1980).

[79] R. Behrends, R. Finkelstein, and A. Sirlin, "Radiative corrections to decay processes," Phys.Rev. **101**, 866 (1956).

[80] S. Berman, "Radiative corrections to muon and neutron decay," Phys.Rev. **112**, 267 (1958).

[81] T. Kinoshita and A. Sirlin, "Radiative corrections to Fermi interactions," Phys.Rev. **113**, 1652 (1959).

[82] M. Roos and A. Sirlin, "Remarks on the radiative corrections of order alpha-squared to muon decay and the determination of g(mu)," Nucl.Phys. **B29**, 296 (1971).

[83] T. van Ritbergen and R. G. Stuart, "On the precise determination of the Fermi coupling constant from the muon lifetime," Nucl.Phys. **B564**, 343 (2000), hep-ph/9904240.

[84] T. van Ritbergen and R. G. Stuart, "Complete two loop quantum electrodynamic contributions to the muon lifetime in the Fermi model," Phys.Rev.Lett. **82**, 488 (1999), hep-ph/9808283.

[85] T. van Ritbergen and R. G. Stuart, "Hadronic contributions to the muon lifetime," Phys.Lett. **B437**, 201 (1998), hep-ph/9802341.

[86] M. Steinhauser and T. Seidensticker, "Second order corrections to the muon lifetime and the semileptonic B decay," Phys.Lett. **B467**, 271 (1999), hep-ph/9909436.

[87] A. Pak and A. Czarnecki, "Mass effects in muon and semileptonic $b \to c$ decays," Phys.Rev.Lett. **100**, 241807 (2008), 0803.0960.

[88] A. Ferroglia, G. Ossola, and A. Sirlin, "Considerations concerning the radiative corrections to muon decay in the Fermi and standard theories," Nucl.Phys. **B560**, 23 (1999), hep-ph/9905442.

[89] T. Lee and C.-N. Yang, "Possible Nonlocal Effects in μ Decay," Phys.Rev. **108**, 1611 (1957).

[90] S. Eckstein and R. Pratt, "Radiative muon decay," Ann.Phys. **8**, 297 (1959).

[91] Q. Ho-Kim and X.-Y. Pham, *Elementary particles and their interactions* (Springer, 1998).

[92] M. Krawczyk and D. Temes, "2HDM(II) radiative corrections in leptonic tau decays," Eur.Phys.J. **C44**, 435 (2005), hep-ph/0410248.

[93] D. Asner, T. Barnes, J. Bian, I. Bigi, N. Brambilla, et al., "Physics at BES-III," Int.J.Mod.Phys. **A24**, S1 (2009), 0809.1869.

[94] S. Berman and A. Sirlin, "Some considerations on the radiative corrections to muon and neutron decay," Ann.Phys. **20**, 20 (1962).

[95] J. Beringer et al. (Particle Data Group), "Review of Particle Physics (RPP)," Phys.Rev. **D86**, 010001 (2012).

[96] A. Sirlin and A. Ferroglia, "Radiative Corrections in Precision Electroweak Physics: a Historical Perspective," Rev.Mod.Phys. **85**, 263 (2013), 1210.5296.

[97] W. Marciano and A. Sirlin, "Electroweak Radiative Corrections to tau Decay," Phys.Rev.Lett. **61**, 1815 (1988).

[98] S. Actis et al. (Working Group on Radiative Corrections and Monte Carlo Generators for Low Energies), "Quest for precision in hadronic cross sections at low energy: Monte Carlo tools vs. experimental data," Eur.Phys.J. **C66**, 585 (2010), 0912.0749.

[99] T. Kinoshita and A. Sirlin, "Muon Decay with Parity Nonconserving Interactions and Radiative Corrections in the Two-Component Theory," Phys.Rev. **107**, 593 (1957).

[100] A. Arbuzov, "First order radiative corrections to polarized muon decay spectrum," Phys.Lett. **B524**, 99 (2002), hep-ph/0110047.

[101] A. Arbuzov, A. Czarnecki, and A. Gaponenko, "Muon decay spectrum: Leading logarithmic approximation," Phys.Rev. **D65**, 113006 (2002), hep-ph/0202102.

[102] A. Arbuzov and K. Melnikov, "$O(\alpha^2 \ln(m_\mu/m_e)$ corrections to electron energy spectrum in muon decay," Phys.Rev. **D66**, 093003 (2002), hep-ph/0205172.

[103] A. Arbuzov, "Higher order QED corrections to muon decay spectrum," JHEP **0303**, 063 (2003), hep-ph/0206036.

[104] C. Anastasiou, K. Melnikov, and F. Petriello, "The Electron energy spectrum in muon decay through $O(\alpha^2)$," JHEP **0709**, 014 (2007), hep-ph/0505069.

[105] A. I. Davydychev, K. Schilcher, and H. Spiesberger, "Hadronic corrections at $O(\alpha^2)$ to the energy spectrum of muon decay," Eur.Phys.J. **C19**, 99 (2001), hep-ph/0011221.

[106] M. Fischer, S. Groote, J. Korner, and M. Mauser, "Leptonic mu and tau decays: Mass effects, polarization effects and O(alpha) radiative corrections," Phys.Rev. **D67**, 113008 (2003), hep-ph/0203048.

[107] D. Webber et al. (MuLan Collaboration), "Measurement of the Positive Muon Lifetime and Determination of the Fermi Constant to Part-per-Million Precision," Phys.Rev.Lett. **106**, 041803 (2011), 1010.0991.

[108] T. Aoyama, M. Hayakawa, T. Kinoshita, and M. Nio, "Tenth-Order QED Contribution to the Electron g-2 and an Improved Value of the Fine Structure Constant," Phys.Rev.Lett. **109**, 111807 (2012), 1205.5368.

[109] C. Fronsdal and H. Uberall, "mu-Meson Decay with Inner Bremsstrahlung," Phys.Rev. **113**, 654 (1959).

[110] Y. Kuno and Y. Okada, "Muon decay and physics beyond the standard model," Rev.Mod.Phys. **73**, 151 (2001), hep-ph/9909265.

[111] A. Fischer, T. Kurosu, and F. Savatier, "QED one loop correction to radiative muon decay," Phys.Rev. **D49**, 3426 (1994).

[112] A. Arbuzov and E. Scherbakova, "One loop corrections to radiative muon decay," Phys.Lett. **B597**, 285 (2004), hep-ph/0404094.

[113] G. Passarino and M. Veltman, "One Loop Corrections for e^+e^- Annihilation Into $\mu^+\mu^-$ in the Weinberg Model," Nucl.Phys. **B160**, 151 (1979).

[114] R. Mertig, M. Bohm, and A. Denner, "FEYN CALC: Computer algebraic calculation of Feynman amplitudes," Comput.Phys.Commun. **64**, 345 (1991).

[115] J. Vermaseren, "New features of FORM," (2000), math-ph/0010025.

[116] G. 't Hooft and M. Veltman, "Scalar One Loop Integrals," Nucl.Phys. **B153**, 365 (1979).

[117] T. Hahn and M. Perez-Victoria, "Automatized one loop calculations in four-dimensions and D-dimensions," Comput.Phys.Commun. **118**, 153 (1999), hep-ph/9807565.

[118] R. K. Ellis and G. Zanderighi, "Scalar one-loop integrals for QCD," JHEP **0802**, 002 (2008), 0712.1851.

[119] I. Mohammad and A. Donnachie, "Higher Order Corrections to Radiative Muon Decay in the Weinberg-Salam Model," (1976).

[120] T. Kinoshita and A. Sirlin, "Radiative Decay of the Muon," Phys. Rev. Lett. **2**, 177 (1959).

[121] T. Kinoshita, "Mass singularities of Feynman amplitudes," J.Math.Phys. **3**, 650 (1962).

[122] T. Lee and M. Nauenberg, "Degenerate Systems and Mass Singularities," Phys.Rev. **133**, B1549 (1964).

[123] R. Crittenden, W. Walker, and J. Ballam, "Radiative decay modes of the muon," Phys.Rev. **121**, 1823 (1961).

[124] J. Adam et al. (MEG Collaboration), "Measurement of polarized muon radiative decay," (2013), 1312.3217.

[125] T. Bergfeld et al. (CLEO Collaboration), "Observation of radiative leptonic decay of the tau lepton," Phys.Rev.Lett. **84**, 830 (2000), hep-ex/9909050.

[126] T. Hahn, "CUBA: A Library for multidimensional numerical integration," Comput.Phys.Commun. **168**, 78 (2005), hep-ph/0404043.

[127] S. Eidelman, D. Epifanov, M. Fael, L. Mercolli, C. Ng, F. Okazawa, and M. Passera, in preparation (2014).

[128] S. Jadach, B. Ward, and Z. Was, "The Precision Monte Carlo event generator K K for two fermion final states in e+ e- collisions," Comput.Phys.Commun. **130**, 260 (2000), hep-ph/9912214.

[129] S. Jadach, Z. Was, R. Decker, and J. H. Kuhn, "The tau decay library TAUOLA: Version 2.4," Comput.Phys.Commun. **76**, 361 (1993).

[130] E. Barberio and Z. Was, "PHOTOS: A Universal Monte Carlo for QED radiative corrections. Version 2.0," Comput.Phys.Commun. **79**, 291 (1994).

[131] R. Brun and *et al.*, "GEANT 3.21," CERN Report No. DD/EE/84-1 (1984).

[132] A. Abashian, K. Gotow, N. Morgan, L. Piilonen, S. Schrenk, et al., "The Belle Detector," Nucl.Instrum.Meth. **A479**, 117 (2002).

[133] J. Brodzicka et al. (Belle Collaboration), "Physics Achievements from the Belle Experiment," PTEP **2012**, 04D001 (2012), 1212.5342.

[134] K. Akai, N. Akasaka, A. Enomoto, J. Flanagan, H. Fukuma, et al., "Commissioning of KEKB," Nucl.Instrum.Meth. **A499**, 191 (2003).

[135] T. Abe, K. Akai, N. Akasaka, M. Akemoto, A. Akiyama, et al., "Achievements of KEKB," PTEP **2013**, 03A001 (2013).

[136] Y.-S. Tsai, "Decay Correlations of Heavy Leptons in $e^+e^- \to l^+l^-$," Phys.Rev. **D4**, 2821 (1971).

[137] W. Fetscher, "Leptonic tau decays: How to determine the Lorentz structure of the charged leptonic weak interaction by experiment," Phys.Rev. **D42**, 1544 (1990).

[138] K. Tamai, "Correlated decay rates of a tau pair for the Michel parameter measurement," Nucl.Phys. **B668**, 385 (2003).

[139] J. Urheim (CLEO Collaboration), "The hadronic current in tau lepton decay to two pseudoscalar mesons," Nucl.Phys.Proc.Suppl. **55C**, 359 (1997).

[140] T. Abe et al. (Belle-II Collaboration), "Belle II Technical Design Report," (2010), 1011.0352.

[141] G. Aad et al. (ATLAS Collaboration), "Observation of a new particle in the search for the Standard Model Higgs boson with the ATLAS detector at the LHC," Phys.Lett. **B716**, 1 (2012), 1207.7214.

[142] S. Chatrchyan et al. (CMS Collaboration), "Observation of a new boson at a mass of 125 GeV with the CMS experiment at the LHC," Phys.Lett. **B716**, 30 (2012), 1207.7235.

[143] T. Aaltonen et al. (CDF Collaboration), "Evidence for $t\bar{t}\gamma$ Production and Measurement of $\sigma_{t\bar{t}}\gamma/\sigma_{t\bar{t}}$," Phys.Rev. **D84**, 031104 (2011), 1106.3970.

[144] C. Collaboration (CMS Collaboration), "Measurement of the inclusive top-quark pair + photon production cross section in the muon + jets channel in pp collisions at 8 TeV,", CMS-PAS-TOP-13-011 (2014).

[145] A. Collaboration (ATLAS Collaboration), "Measurement of the inclusive $t\bar{t}\gamma$ cross section with the ATLAS detector,", ATLAS-CONF-2011-153 (2011).

[146] W. Hollik, "Radiative Corrections in the Standard Model and their Role for Precision Tests of the Electroweak Theory," Fortsch.Phys. **38**, 165 (1990).

[147] J. Bernabeu, J. Vidal, and G. Gonzalez-Sprinberg, "The Weak magnetic moment of heavy quarks," Phys.Lett. **B397**, 255 (1997), hep-ph/9702222.

[148] W. Bernreuther, R. Bonciani, T. Gehrmann, R. Heinesch, T. Leineweber, et al., "Two-loop QCD corrections to the heavy quark form-factors: The Vector contributions," Nucl.Phys. **B706**, 245 (2005), hep-ph/0406046.

[149] W. Bernreuther, R. Bonciani, T. Gehrmann, R. Heinesch, T. Leineweber, et al., "Two-loop QCD corrections to the heavy quark form-factors: Axial vector contributions," Nucl.Phys. **B712**, 229 (2005), hep-ph/0412259.

[150] W. Bernreuther, R. Bonciani, T. Gehrmann, R. Heinesch, T. Leineweber, et al., "Two-loop QCD corrections to the heavy quark form-factors: Anomaly contributions," Nucl.Phys. **B723**, 91 (2005), hep-ph/0504190.

[151] W. Bernreuther, R. Bonciani, T. Gehrmann, R. Heinesch, T. Leineweber, et al., "QCD corrections to static heavy quark form-factors," Phys.Rev.Lett. **95**, 261802 (2005), hep-ph/0509341.

[152] A. Grozin, P. Marquard, J. Piclum, and M. Steinhauser, "Three-Loop Chromomagnetic Interaction in HQET," Nucl.Phys. **B789**, 277 (2008), 0707.1388.

[153] E. Shabalin, "Electric Dipole Moment of Quark in a Gauge Theory with Left-Handed Currents," Sov.J.Nucl.Phys. **28**, 75 (1978).

[154] I. Khriplovich, "Quark Electric Dipole Moment and Induced θ Term in the Kobayashi-Maskawa Model," Phys.Lett. **B173**, 193 (1986).

[155] T. Ibrahim and P. Nath, "The Top quark electric dipole moment in an MSSM extension with vector like multiplets," Phys.Rev. **D82**, 055001 (2010), 1007.0432.

[156] T. Ibrahim and P. Nath, "The Chromoelectric Dipole Moment of the Top Quark in Models with Vector Like Multiplets," Phys.Rev. **D84**, 015003 (2011), 1104.3851.

[157] D. Atwood, S. Bar-Shalom, G. Eilam, and A. Soni, "CP violation in top physics," Phys.Rept. **347**, 1 (2001), hep-ph/0006032.

[158] J. Aguilar-Saavedra, "A Minimal set of top anomalous couplings," Nucl.Phys. **B812**, 181 (2009), 0811.3842.

[159] C. Zhang and S. Willenbrock, "Effective-Field-Theory Approach to Top-Quark Production and Decay," Phys.Rev. **D83**, 034006 (2011), 1008.3869.

[160] J. Aguilar-Saavedra, M. Fiolhais, and A. Onofre, "Top Effective Operators at the ILC," JHEP **1207**, 180 (2012), 1206.1033.

[161] B. Grzadkowski, Z. Hioki, K. Ohkuma, and J. Wudka, "Probing anomalous top quark couplings induced by dimension-six operators at photon colliders," Nucl.Phys. **B689**, 108 (2004), hep-ph/0310159.

[162] M. Fael and T. Gehrmann, "Probing top quark electromagnetic dipole moments in single-top-plus-photon production," Phys.Rev. **D88**, 033003 (2013), 1307.1349.

[163] M. Czakon, P. Fiedler, and A. Mitov, "The total top quark pair production cross-section at hadron colliders through $O(\alpha_S^4)$," Phys.Rev.Lett. **110**, 252004 (2013), 1303.6254.

[164] N. Kidonakis, "Next-to-next-to-leading-order collinear and soft gluon corrections for t-channel single top quark production," Phys.Rev. **D83**, 091503 (2011), 1103.2792.

[165] D. Peng-Fei, Z. Ren-You, M. Wen-Gan, H. Liang, G. Lei, et al., "Next-to-leading order QCD corrections to $t\bar{t}\gamma$ production at the 7 TeV LHC," Chin.Phys.Lett. **28**, 111401 (2011), 1110.2315.

[166] K. Melnikov, M. Schulze, and A. Scharf, "QCD corrections to top quark pair production in association with a photon at hadron colliders," Phys.Rev. **D83**, 074013 (2011), 1102.1967.

[167] J. Alwall, M. Herquet, F. Maltoni, O. Mattelaer, and T. Stelzer, "MadGraph 5 : Going Beyond," JHEP **1106**, 128 (2011), 1106.0522.

[168] S. Chatrchyan et al. (CMS Collaboration), "Measurement of the single-top-quark t-channel cross section in pp collisions at $\sqrt{s} = 7$ TeV," JHEP **1212**, 035 (2012), 1209.4533.

[169] G. Aad et al. (ATLAS Collaboration), "Measurement of the t-channel single top-quark production cross section in pp collisions at $\sqrt{s} = 7$ TeV with the ATLAS detector," Phys.Lett. **B717**, 330 (2012), 1205.3130.

[170] T. Hahn, "Generating Feynman diagrams and amplitudes with FeynArts 3," Comput.Phys.Commun. **140**, 418 (2001), hep-ph/0012260.

[171] N. D. Christensen and C. Duhr, "FeynRules - Feynman rules made easy," Comput.Phys.Commun. **180**, 1614 (2009), 0806.4194.

[172] J. Pumplin, D. Stump, J. Huston, H. Lai, P. M. Nadolsky, et al., "New generation of parton distributions with uncertainties from global QCD analysis," JHEP **0207**, 012 (2002), hep-ph/0201195.

[173] J. Bauer, "Prospects for the Observation of Electroweak Top Quark Production with the CMS Experiment,", CERN-THESIS-2010-146 (2010).

[174] S. Chatrchyan et al. (CMS Collaboration), "Identification of b-quark jets with the CMS experiment," JINST **8**, P04013 (2013), 1211.4462.

[175] G. Aad et al. (ATLAS Collaboration), "Measurements of $W\gamma$ and $Z\gamma$ production in pp collisions at $\sqrt{s}$= 7 TeV with the ATLAS detector at the LHC," Phys.Rev. **D87**, 112003 (2013), 1302.1283.

[176] G. Aad et al. (ATLAS Collaboration), "Expected Performance of the ATLAS Experiment - Detector, Trigger and Physics," (2009), 0901.0512.

[177] G. Aad et al. (ATLAS Collaboration), "Measurement of isolated-photon pair production in pp collisions at $\sqrt{s} = 7$ TeV with the ATLAS detector," JHEP **1301**, 086 (2013), 1211.1913.

[178] J. Aguilar-Saavedra et al. (ECFA/DESY LC Physics Working Group), "TESLA: The Superconducting electron positron linear collider with an integrated x-ray laser laboratory. Technical design report. Part 3. Physics at an e+ e- linear collider," (2001), hep-ph/0106315.

[179] D. Asner, A. Hoang, Y. Kiyo, R. Pöschl, Y. Sumino, et al., "Top quark precision physics at the International Linear Collider," (2013), 1307.8265.

[180] M. Amjad, M. Boronat, T. Frisson, I. Garcia, R. Poschl, et al., "A precise determination of top quark electro-weak couplings at the ILC operating at $\sqrt{s} = 500$ GeV," (2013), 1307.8102.